The cation channel mechanisms of subthreshold inward depolarizing currents in the VTA dopaminergic neurons and their roles in the depression-like behavior

Jing Wang[1,3], Min Su[1,4], Dongmei Zhang[1,5], Ludi Zhang[1], Chenxu Niu[1], Chaoyi Li[1], Shuangzhu You[1], Yuqi Sang[1], Yongxue Zhang[1,6], Xiaona Du[1], Hailin Zhang[1,2*]

[1]Department of Pharmacology; The Key Laboratory of Neural and Vascular Biology, Ministry of Education; The Key Laboratory of New Drug Pharmacology and Toxicology, Hebei Medical University, Shijiazhuang, Hebei, China
[2]Department of Psychiatry, The First Hospital of Hebei Medical University, Mental Health Institute of Hebei Medical University, China
[3]Department of Pharmacochemistry, Hebei University of Chinese Medicine, Shijiazhuang, Hebei, China
[4]Yiling Pharmaceutical Company, Shijiazhuang, Hebei, China
[5]Department of Clinical Pharmacy, Xintai Ninth Hoapital, Xintai, Hebei, China
[6]Department of Pharmacy, Handan First Hospital, Handan, Hebei, China

*** Correspondence:**
Hailin Zhang
zhanghl@hebmu.edu.cn

Abstract:

The slow-intrinsic-pacemaker dopaminergic (DA) neurons originating in the ventral tegmental area (VTA) is implicated in various mood- and emotion-related disorders, such as anxiety, fear, stress and depression. Abnormal activity of projection-specific VTA DA neurons is the key factor in the development of these disorders. Here, we describe the crucial role for the NALCN and TRPC6, non-selective cation channels in mediating the subthreshold inward depolarizing current and driving the firing of action potentials of VTA DA neurons in physiological condition. Otherwise, we demonstrate that downregulation of TRPC6 protein expression in the VTA DA neurons likely contributes to the reduced activity of projection-specific VTA DA neuron in CMUS depressive mice. Furthermore, selective knockdown of TRPC6 channels in the VTA DA neurons conferred mice with depression-like behavior. This current study suggests down-regulation of TRPC6 expression/function is involved in reduced VTA DA neuron firing and depression-like behavior in the mouse models of

depression.

Keywords: Ventral tegmental area, Dopaminergic neurons, Cation channels, NALCN, TRPC6 channel

Introduction

Dopaminergic (DA) neurons in the ventral tegmental area (VTA) play a key role in mood, reward and addictive behaviors[1]. These DA neurons project, through mesocorticolimbic dopaminergic system, to brain regions including the nucleus accumbens (NAc), medial prefrontal cortex (mPFC) and basolateral amygdala (BLA), and modulate these target neuronal circuits through their regulated activity (firing of action potentials)[2, 3]. As such, understandably, the altered functional activity of the VTA DA neurons is found to be the key determinants in abnormal behaviors related to the diseased conditions such as depression states[4]. Thus, the mechanism underlying the firing activity of the VTA DA neurons is crucial for understanding the function of the DA circuitry and the pathogenesis of related mental diseases[4-8].

The VTA DA neurons are slow intrinsic pacemakers, which are further modulated by synaptic inputs from multiple excitatory and inhibitory projections[9, 10]. Firing activity controls the release of DA, thus function of the VTA DA neurons. The altered activity of the VTA DA neurons in a pathological state includes altered firing frequency and switch of the firing patterns[7, 11].

Mechanism for spontaneous firing of action potential (AP) is the key to understand functional regulation of the VTA DA neurons. A variety of ion channels (e.g. voltage-gated Na^+ channels, high-threshold-activated Ca^{2+} channels, Kv2, large conductance calcium-activated potassium channels, A- and M-type potassium channels) are reported to be involved in regulation of the autonomic firing activity of midbrain DA neurons (including the substantial nigra compact par, SNc and VTA)[12-22]. However, it is not completely clear how this spontaneous firing is initiated. AP fires when the resting membrane potential (RMP) is depolarized to the activation threshold for the voltage-dependent Na^+ channels, which results in opening of Na^+ channel and the upstroke of AP[12]. Therefore, a controlled depolarization of the RMP to the activation threshold of AP is the first key step in a cascade leading to firing of AP. In

the VTA DA neurons, the identity of ion channels contributing to this subthreshold depolarization has not been unambiguously established.

In some cells with spontaneous firing of AP, such as cardiomyocytes and certain neurons (including a subset of midbrain SNc DA neurons[23]), the ionic mechanism for the auto-rhythmicity is the HCN, a non-selective cation channel that would depolarize the membrane potential after being activated at a hyperpolarized membrane potential[23]. However, in the VTA DA neurons, results concerning the HCN channels to the spontaneous firing are controversial[15, 23-25].

Another non-selective cation channel, NALCN, which unlike HCN, is a non-voltage dependent channel[26], and is reported to be among the candidates for molecular correlates of the persistent background Na^+ leak currents in the VTA DA neurons [27, 28]. The NALCN-mediated background Na^+ leak currents are found to be involved in modulation of firing activity in a variety of neurons including DA neurons in the SNc[26, 28-31]. However, it has not been reported if NALCN play a role in spontaneous firing of the VTA DA neurons, although the VTA DA neurons have larger Na^+ leak currents than SNc DA neurons do [15].

TRP channels are a large class of non-selective cation channels, and are widely distributed in the peripheral and central nervous system. TRPC3, which has a high homology with TRPC6[32], is found to be involved in the regulation of cardiac and SNc DA neuronal excitability, generating depolarizing currents, triggering action potentials and participating in cellular rhythmic firing[31, 33, 34]. The role of TRP channels in the regulation of VTA DA neuronal excitability has not been described.

In this study, we drove to find channel conductance which contribute to the subthreshold depolarization and thus the spontaneous firing of the VTA DA neurons. And further more we investigated if these channels are the molecular mechanism for the altered function activity of the VTA DA neurons related to depression-like behaviors in mouse model of depression. We started by profiling the expression of non-selective cation channels (NSCCs) of the VTA DA neurons using method of Patch-Seq from midbrain DA neurons projecting to different brain regions, and then focused on HCN, NALCN, TRPC6 and TRPV2 channels which are dominantly expressed in these DA neurons.

Results

Inflow of extracellular Na^+ contribute to the subthreshold depolarization of the VTA DA neurons

One key feature of the midbrain DA neurons is that these neurons are relatively depolarized in the resting condition; the resting membrane potential (RMP) is far from the K^+ equilibrium potential (~-55 mV *vs* ~-90 mV)[15], which enable the spontaneous firing possibly. Thus there must exist persistent inward depolarizing conductance counterbalancing the hyperpolarizing K^+ conductance which otherwise would maintain the RMP at a hyperpolarized level. The main aim of this study is to identify the subthreshold depolarizing conductances which contribute to the spontaneous firing of the VTA DA neurons. For this, we first observed firing frequency and the RMP of the VTA DA neurons using patch clamp recordings. The midbrain DA neurons, marked by dopamine transporter (DAT), mainly located in the VTA and SNc (**Fig. 1Ai**). We recorded neurons from the VTA brain slices of mice, and performed single-cell PCR post electrophysiologic recordings to identify the DA neurons with established markers for DA neurons (TH, DAT, D_2R (type 2 dopamine receptor), and GIRK2 (G protein-gated inward rectifier K inwardly rectifying K^+ channels)). Although the majority of cells in the VTA area are DA neurons (~60%), there are still about 30% GABA neurons and a small number of glutamatergic neurons [35, 36]. Glutamatergic- and GABAergic neurons were also single-cell PCR typed by using markers of vGluT2 (vesicular glutamate transporter 2) and GAD1 (glutamic acid decarboxylase 1), respectively (**Fig. 1Aii**).

To focus on the intrinsic channel conductance for spontaneous firing, potential input modulation from fast-type transmitter transmission to the VTA DA neurons, namely activation of AMPA/kainite/NMDA receptor and $GABA_A$ receptor were blocked by receptor antagonists CNQX, DL-AP5 and picrotoxin [15], respectively, in the following experiments.

We first studied whether inflow of extracellular Ca^{2+} contributed to initiation of spontaneous firing in the VTA DA neurons. It has been shown that, unlike the SNc DA neurons, the VTA DA neurons do not have subthreshold Ca^{2+} oscillatory waves [15], suggesting that subthreshold Ca^{2+} should not be an important component of

127 subthreshold depolarizing conductance in the VTA DA neurons. In line with this
128 finding, we found in our study, replacing Ca^{2+} with Mg^{2+} from the extracellular
129 recording solution (ACSF, artificial cerebral spinal solution) did not reduce, but rather
130 instead, increased the firing frequency of the VTA DA neurons (**Fig. 1B**, from 1.90 ±
131 0.22 Hz to 3.05 ± 0.33 Hz, n = 6, $P < 0.001$). In consistent with this，the RMP of the
132 VTA DA neurons was also not affected by replacing Ca^{2+} with Mg^{2+} from ACSF (**Fig.**
133 **1C**, from -50.76 ± 1.16 mV to -48.83 ± 1.76 mV, n = 6, $P > 0.05$).
134 We then, in comparison with Ca^{2+}, observed the role of extracellular Na^{+} in the RMP
135 of the VTA DA neurons. For this, we followed the method of a previous study[15], by
136 replacing Na^{+} in ACSF with NMDG (N-methyl-d-glucamine); TTX (Tetrodotoxin)
137 was also added to block the TTX-sensitive Na^{+} currents, which is known to be the
138 main contributor to the suprathreshold depolarization component of the action
139 potential. Replacement of the extracellular Na^{+} with NMDG resulted in a
140 hyperpolarization of the RMP, from -46.00 ± 2.92 mV to -66.80 ± 1.53 mV (n = 5, $P <$
141 0.05, **Figure 1D**), indicating a persistent inflow of Na^{+} through a TTX-insensitive
142 conductance which caused significant depolarization of the neurons, contributing
143 significantly to the subthreshold depolarization of the VTA DA neurons.
144 Taken together, above results indicate persistent Na^{+} influx contribute to the
145 subthreshold depolarization of the VTA DA neurons.
146
147 **Potential candidates of channel conductance contributing to subthreshold**
148 **depolarization of the VTA DA neurons**
149 The channel conductance mediating the above-described persistent Na^{+} influx should
150 come from a cation channel(s) permeating to Na^{+}. We thus investigated the presence
151 and expression level of non-selective cation channels (NSCCs) in the VTA DA
152 neurons using a combination of patch clamp and single-cell RNA-Seq (Patch-seq)
153 technology[37]. In this part of the study, we considered the heterogeneity and
154 projection-specificity of the VTA DA neurons, i.e. VTA DA neurons projecting to
155 different brain regions have different electrophysiological characteristics[38]. Using
156 retrograde labelling techniques using retrobeads, sixty VTA neurons projecting to five
157 different brain regions (medial prefrontal cortex, mPFC; basal lateral amygdala, BLA;

158 nucleus accumben core, NAc c; nucleus accumben lateral shell, NAc ls; nucleus
159 accumben medial shell, NAc ms) (**sFig.1**) were collected for RNA-Seq, using
160 patch-clamp electrodes. Consistent with previous study[38], the VTA DA neurons
161 projected to above different brain regions were anatomically congregated into
162 subregions of the VTA (**sFig.2)**. The high expression of biomarkers (TH, Ddc and
163 DAT) in the 45 cells of 60 cells (**Fig. 2A**) indicates that these are DA neurons. In
164 addition, a significant proportion of neurons (predominantly those projecting to NAc
165 ms, BLA, and mPFC) have biomarkers (VGluT1-3) of glutamatergic neurons,
166 predicting a possible coexistence of neurotransmitters (DA and glutamate)[39]. In
167 contrast, fewer GABAergic neuronal markers (GAD1/2 and VGAT) co-expressed
168 with the DA neurons, which is consistent with previous studies that VTA DA neurons
169 coexpressing GABAergic neuronal markers mainly project to the lateral habenula[40]. It
170 needs to be noted that some neurons in the VTA only expressed markers for
171 glutamatergic or GABAergic neurons, these neurons were excluded from further
172 analysis as we focused our study on the DA neurons.
173 Expression files of NSCCs in the VTA DA neurons classified by projection specificity
174 were analyzed and shown in **Fig. 2B**. Different colored strips on the top of the figure
175 corresponded to the projection specificity coded by the same colors in **Fig. 2A**.
176 Multiple transient receptor potential channels (TRP) were present in the VTA DA
177 neurons, with prominent expression level of TRPC6 and TRPV2 (**Fig. 2Bi**). Other
178 prominently expressed NSCCs included HCN2, HCN3, NALCN and pannexin 1
179 (Panx1) (**Fig. 2Bii**). Summarized averaged relative expression levels for eight most
180 richly expressed NSCCs were shown in **Fig. 2Biii**. Furthermore, projection-specific
181 expression of these dominantly expressed NSCCs were analyzed and shown in **Fig 2C**;
182 interestingly only TRPC6 seemed expressed in a projection-specific manner, namely,
183 the VTA DA neurons projecting to the NAc have higher TRPC6 expression than the
184 VTA DA neurons projecting to the BLA and the mPFC **(Fig 2C**). In our subsequent
185 study, we focused our study on HCN, NALCN, TRPC6 and TRPV2, one for they are
186 the prominently expression channels, and two for some of these channels have been
187 indicated in modulation of excitability of different neuron types[23, 24, 26, 28-31, 41]. Panx1
188 was investigated in a separate study since it normally composes the semi channels

189 which are different from these more conventional ion channels.

190

191 **HCN does not contribute to the spontaneous firing of the VTA DA neurons**

192 We mainly used two pharmacological tools of HCN channel blockers, CsCl and
193 ZD7288[15, 24] to explore the role of HCN channels in the spontaneous firing of the
194 VTA DA neurons. Efficient blocking effect of these blockers on HCN channel were
195 first verified. For this, the sag potential produced by a hyperpolarizing current (-100
196 pA) injection was used to assess HCN activity[24]. Both CsCl (3 mM) and ZD7288 (60
197 μM) effectively reduced the sag potential (from 16.43 ± 2.96 mV to 3.84 ± 1.92 mV, n
198 = 4, P < 0.05; from 19.38 ± 3.14 mV to 4.18 ± 2.60 mV, n = 4, respectively, P < 0.05)
199 (**sFig. 3A and B**).

200 However, these same HCN blockers did not inhibit the spontaneous firing of the VTA
201 DA neurons; CsCl slightly increased (1.96 ± 0.19 Hz to 2.14 ± 0.34 Hz, n = 7)
202 whereas ZD7288 slightly decreased the firing frequency (1.65 ± 0.25 Hz to 1.50 ±
203 0.24 Hz, n = 13), but none of these effects were statistically significant (*P* > 0.05)
204 (**sFig. 3C and D)**. It has been reported that VTA DA neurons projecting to the NAc
205 lateral shell have more pronounced HCN/Ih currents than other VTA DA neurons [38].
206 However, even the VTA DA neurons projecting to the NAc lateral shell (retrogradely
207 labelled by retrobeads), no effect of CsCl or ZD7288 on the spontaneous firing of the
208 VTA DA neurons were observed (from 2.04 ± 0.24 Hz to 1.93 ± 0.22 Hz, n = 5, by
209 CsCl, and from 1.71 ± 0.29 Hz to 1.65 ± 0.33 Hz, n = 5, by ZD7288, *P* > 0.05) (**sFig.
210 4**).

211 HCN are activated by membrane hyperpolarization, with an activation threshold
212 around -70~-90 mV (HCN2, HCN3)[42, 43]. At a depolarized RMP like these in the VTA
213 DA neurons (-51.28 ± 1.85 mV, n = 8; e.g. -54.50 mV, **sFig 3Ai**, and -53.50mV, **sFig.
214 3Bi**), HCH are mostly likely not activated thus would not participate in generation of
215 spontaneous firing. To further prove this, we tested if a more hyperpolarized RMP
216 would involve HCN in the spontaneous firing of the VTA DA neurons. For this, we
217 first lowered the K^+ concentration in the extracellular ACSF from 3 mM to 1.5 mM to
218 increase the gradient between inside and outside cellular K^+; this maneuver indeed
219 hyperpolarized the cell membrane from -55.00 ± 2.74 mV to -66.40 ± 3.28 mV (n = 5,

220 $P < 0.05$ mV) (**sFig. 4C**). Interestingly, under 1.5 mM extracellular K^+, the
221 spontaneous firing of the VTA DA neurons was almost totally blocked by ZD7288
222 (**sFig. 4D**), although an initial enhancement was seen in some neurons (**sFig. 4Di**).
223 We tested another possible mechanism for HCN's failure to participate in generation
224 of VTA DA firing. It has been reported that in the midbrain SNc DA neurons, HCN is
225 involved in the spontaneous firing in young but not in adult mice, due to a more
226 hyperpolarization-shifted activation threshold of HCN in SNc DA neurons in adult
227 mice. We tested if this could also be the case in the VTA DA neurons. Indeed, as
228 shown in **sFig. 4E**, in contrast to what we saw in adult mice, the spontaneous firing
229 frequency of the VTA DA neurons in young mice (less than 15 days postnatal) was
230 significantly reduced by ZD7288 (from 1.86 ± 0.29 Hz to 0.98 ± 0.24 Hz, n = 9, $P <$
231 0.01).
232 Taken together, above results suggest HCN is not involved in the spontaneous firing
233 of the VTA DA neurons in adult mice, due to a depolarized RMP and a
234 hyperpolarization-shifted activation property.
235
236 **NALCN contributes to subthreshold depolarization and spontaneous firing of**
237 **the VTA DA neurons**
238 The Na^+ currents produced by NALCN have been suggested to be an important
239 component of background Na^+ currents in multiple central neurons including DA
240 neurons in the substantia nigra[28]. We next investigated if NALCN also play a role in
241 setting the RMP and in the spontaneous firing of the VTA DA neurons. In consistent
242 with above RNA-Seq results, both immunofluorescence (**Fig. 3A**) and single-cell
243 PCR (**Fig. 3B)** results confirmed broad expression of NALCN in the VTA DA
244 neurons.
245 $GdCl_3$ (100 μM), a nonspecific NALCN blocker [29, 30], depolarized the RMP of the
246 VTA DA neurons from -53.60 ± 4.78 mV to -67.80 ± 3.23 mV (n = 5, $P < 0.05$) (**Fig.**
247 **3C**), reduced the spontaneous firing frequency of the VTA DA neurons from 1.89 ±
248 0.29 Hz to 1.32 ± 0.37 Hz (n = 7, $P < 0.01$) (**Fig. 3D**).
249 To observe a more specific effect on NALCN, a shRNA against NALCN was used to
250 knockdown NALCN. For this, AAV9 viral construct (AAV9-U6-

shRNA(NALCN)-CMV-GFP) was injected into the VTA of a mouse; similar AAV viral construct containing scramble-shRNA of nonsense sequences was utilized as controls. The qPCR results show sufficient knockdown of NALCN mRNA (NALCN-shRNA: 0.32 ± 0.07, control scramble-shRNA: 1.07 ± 0.19, n = 6, $P < 0.01$, **Fig. 3E**) in the VTA tissue. Immunofluorescence results (**Fig. 3F**) show efficient infection of the VTA DA neurons (GFP expression in the DAT-positive neurons) by the virus. Knockdown of NALCN in the VTA DA neurons by shRNA almost completely silenced the firing of the VTA DA neurons (0.07 ± 0.04 Hz *vs* 1.84 ± 0.25 Hz in shRNA (n = 12) and scramble-shRNA (n = 10) infected VTA DA neurons, respectively, $P < 0.0001$, **Fig. 3G**). Furthermore, the RMP of the VTA DA neurons was significantly hyperpolarized (-60.67 ± 2.33 mV *vs* -48.9 ± 1.45 mV in shRNA and scramble-shRNA infected VTA DA neurons, respectively, n = 18 and 15, $P < 0.0001$, **Fig. 3H**).

Taken together, above results suggest that NALCN is a major contributor to the subthreshold depolarization and contribute significantly to the generation of spontaneous firing in the VTA DA neurons.

TRPC6 contributes to subthreshold depolarization and spontaneous firing of the VTA DA neurons

Above RNA-Seq results suggest a broad and strong expression of TRPC6 and TRPV2 channels in the VTA DA neurons. This part of the experiments was focused on the role of these two TRP channels in subthreshold depolarization and spontaneous firing of the VTA DA neurons.

In consistent with the RNA-Seq results, single-cell PCR experiments confirmed high proportion expression of TRPC6 and TRPV2 in the VTA DA neurons (**Fig. 4A**); among the 28 VTA DA neurons (DAT^+), 20 neurons expressed TRPV2 (71.4%), and 18 neurons (64.3%) expressed TRPC6. TRPC3, which is highly homologous with TRPC6[44] and has been reported to be involved in the firing activity of the SNc DA neurons[31], was not detected in RNA-Seq study (**Fig. 2B**), nor in the single-cell PCR experiment (**Fig. 4A**). These results reciprocally confirmed the reliability of both RNA-Seq and single cell PCR results.

282 General roles of TRP channels in subthreshold depolarization and spontaneous firing
283 of the VTA DA neurons were first assessed using two non-specific broad-spectrum
284 TRP channel blockers, 2-aminoethoxydiphenylborane (2-APB; 100 μM) and
285 flufenamicacid (FFA; 100 μM). Both TRP channel blockers significantly reduced the
286 firing frequency of the VTA DA neurons (2-APB: from 1.32 ± 0.27 Hz to 0.06 ± 0.02
287 Hz, n = 12, $P < 0.001$; FFA: from 1.38 ± 0.17 Hz to 0.52 ± 0.06 Hz, n = 13, $P < 0.001$;
288 **Fig. 4B, 4C**). Accordingly, both blockers also significantly hyperpolarized the RMP
289 of the VTA DA neurons (2-APB: from -51.01 ± 2.20 mV to -61.64 ± 1.28 mV, n = 6,
290 $P < 0.01$; FFA: from -50.50 ± 2.36 mV to -69.65 ± 2.06 mV, n = 6, $P < 0.01$; **Fig. 4D,**
291 **4E**).
292 We then tested a more TRPV channel-specific blocker ruthenium red (RR), to study
293 possible role of TRPV2 (and other TRPV) in the spontaneous firing of the VTA DA
294 neurons. RR (60 μM), on average statistically, did not affect the spontaneous firing of
295 the VTA DA neurons (from 2.30 ± 0.31 Hz to 2.18 ± 0.32 Hz, n = 9, $P > 0.05$) (**sFig.**
296 **5**). However, it needs to be noted that among the nine VTA DA neurons we tested,
297 both increase (**sFig. 5B**) and decrease (**sFig. 5C**) of firing frequency by RR were seen,
298 thus with opposite changes of firing frequency in different populations of neurons
299 (**sFig. 5A**), no overall effect of RR was obtained from the current analysis.
300 We then focused our next study on TRPC6. In consistent with both RNA-Seq (**Fig. 2B**)
301 and single-cell PCR (**Fig. 4A**) results, the mRNA level of TRPC6 in mPFC-projecting
302 VTA single DA neuron is significantly lower than that in NAc c-projecting VTA
303 single DA neuron (0.56 ± 0.12, n = 25 for mPFC-projecting TH-positive cells *vs* 1.09
304 ± 0.10, n = 28 for NAc c-projecting TH-positive cells, ** $P < 0.01$, **Fig. 5A**) The
305 immunofluorescence results also demonstrated strong expression of TRPC6 protein in
306 the VTA DA neurons (**Fig. 5B**, TH-positive). A AAV viral construct with shRNA
307 against TRPC6 (AAV9-U6-shRNA (TRPC6)-CMV-GFP) was injected into the VTA
308 of mice, to knockdown TRPC6; efficiency of this knockdown was assessed by using
309 qPCR measuring the mRNA level of TRPC6 in the VTA tissue (**Fig. 5C**), and
310 efficiency of viral infection into the VTA DA neurons (marked by DAT) was observed
311 through visualization of GFP (**Fig. 5D**). Both qPCR (Fig. **5C**) and
312 immunofluorescence (**Fig. 5D**) results indicated a sufficient repression of TRPC6 in

313 the VTA DA neurons. Indicative of a significant role in the spontaneous firing and
314 subthreshold depolarization, knockdown of TRPC6 (TRPC6-KD) resulted in a
315 substantial reduction in the spontaneous firing frequency (0.80 ± 0.25 Hz, n = 9 for
316 TRPC6-KD *vs* 1.90 ± 0.27 Hz, n = 9 for scramble-shRNA, $P < 0.01$, **Fig. 5E**), and
317 hyperpolarization of the RMP (-58.21 ± 1.79 mV, n = 10 for TRPC6-KD *vs* -50.02 ±
318 0.67 mV, n = 10 scramble-shRNA, $P < 0.001$, **Fig. 5G**) of the VTA DA neurons. In
319 addition, the inhibitory effect of 2-APB on the firing of VTA DA neurons infected
320 with TRPC6-shRNA largely diminished, with no statistical difference in firing
321 frequency before and after dosing (from 0.58 ± 0.15 Hz to 0.40 ± 0.15 Hz, n = 7, $P >$
322 0.05, **Fig. 5F**).
323 Taken together, above results indicate TRPC6 is an important contributor in
324 subthreshold depolarization and spontaneous firing of the VTA DA neurons.
325
326 **Down-regulation of TRPC6 contributes to the altered firing activity of the VTA**
327 **DA neurons in depression model**
328 In multiple depression models, the depression-like behavior was directly linked to the
329 altered firing activity of the VTA DA neurons [10-15]. In consideration of the
330 evidence we described above that NALCN and TRPC6 play key roles in firing
331 activity of the VTA DA neurons, we went further to study if these channels also
332 contributed to the altered firing activity of the VTA DA neurons and to the
333 development of the depression-like behavior in depression models of mice.
334 We first established a mice depression model of chronic mild unpredictable stress
335 (CMUS) [45], which, after 5 weeks subjecting to two different stressors every day (**Fig.**
336 **6A**), manifested depression-like behaviors in the sucrose preference test (SPT) and the
337 tail suspension test (TST) (**Fig. 6B**), with reduced sucrose preference and lengthened
338 immobility time, respectively. Multiple other behaviors tests were also performed on
339 these CMUS mice (**sFig. 6**), all indicating depression/anxiety behaviors.
340 It has been shown that a reduced firing activity in the VTA DA neurons is responsible
341 for the depression-like behavior in the CMUS model[46, 47]. In consistent with this
342 finding, we also found the firing frequency of the VTA DA neurons from the CMUS
343 mice was significantly reduced as compared with that from the control mice (2.83 ±

344 0.42 Hz, n = 18 for control mice *vs* 1.30 ± 0.14 Hz, n = 28 for CMUS mice, $P < 0.01$,
345 **Fig. 6C**). In agreement with a role for TRPC6 in this reduced firing activity, TRPC6
346 protein in the VTA tissue was found to be down-regulated in western blot experiments
347 (**Fig. 6D**). On the other hand, NALCN protein in the VTA was not altered in the
348 CMUS mice model of depression (**sFig. 7**).
349 We also tested if this down-regulation of TRPC6 protein could also be found in a
350 similar but different model of depression. For this, a chronic restraint stress (CRS)
351 model was used. After 3 weeks of restraint stress stimulation, the CRS mice
352 developed similar depression/anxiety behavior in the behavior tests like these
353 similarly performed in the CMUS model (**sFig. 8A-G**). Importantly, mice with
354 CRS-induced depression also showed a significant downregulation of TRPC6 protein
355 in the VTA (0.43 ± 0.09-fold, n = 6 for control and n = 9 for CRS, $P < 0.001$, **sFig.**
356 **8H**).
357 It is known that CMUS mainly decreases the activity of VTA dopamine neurons that
358 project to mPFC[11, 47]. To prove further that the decreased firing activity of the
359 mPFC-projecting VTA DA neurons in the CMUS mice was associated with the
360 down-regulation of TRPC6 expression, we reasoned that a down-regulated TRPC6
361 would play a less role in a reduced firing activity like that found in the CMUS mice,
362 thus the firing activity in these mice would respond less to the TRP channel inhibitors.
363 Indeed, TRP channel inhibitor 2-APB lost its inhibitory effect on the firing activity of
364 the mPFC-projecting VTA DA neurons from the CMUS mice (1.61 ± 0.23Hz to 1.19
365 ± 0.22 Hz, n = 15, $P > 0.05$) but not from the control mice (3.74 ± 0.42 Hz to 0.17 ±
366 0.09 Hz, n = 12, $P < 0.001$) (**Fig. 6E**).
367 Taken together, above results suggest downregulation of TRPC6 is a key determinant
368 for the altered firing activity of the VTA DA neuron in mice models of depression
369
370 **Down-regulation of TRPC6 in the VTA DA neurons confer the mice with**
371 **depression-like behavior**
372 If down-regulation of TRPC6 is crucial for the depression-like behaviors, like that
373 indicated above in the CMUS and the CRS depression models, then down regulation
374 of TRPC6 in non-stressfully treated mice should also develop depression-like

375 behavior. We tested this possibility by selectively knocking down TRPC6 in the VTA
376 DA neurons, using DAT-Cre mice injected with a AAV viral construct
377 (AAV9-hSyn-DIO-shRNA (TRPC6) -RFP) (**Fig. 7A**), driving the expression of
378 shRNA against TRPC6 selectively in the VTA DA neurons. Three weeks after the
379 AAV injection, the qPCR (**Fig. 7B**) and the immunofluorescence results (**Fig. 7C**)
380 indicated an efficient downregulation of TRPC6 in the VTA DA neurons.
381 We next compared the depression- and anxiety-like behaviors in these conditionally
382 TRPC6-knockout mice (TRPC-cKD) with that in the control mice (infected with virus
383 carrying the scrambled shRNA). As shown in **Fig. 7D**, in the TRPC6-cKD mice, the
384 sucrose preference was significantly reduced (7Di, 72.60 ± 3.52 %, n = 13 for
385 TRPC-cKD, *vs* 92.74 ± 0.86 %, n = 9 for control, $P < 0.01$), the immobility time in
386 the TST was significantly lengthened (7Dii, 192.10 ± 3.13 s *vs* 133.20 ± 8.89 s, $P <$
387 0.001), and the time spent in the open arm in the elevated plus maze test was
388 significantly reduced (7Diii, 7.29 ± 1.45 s *vs* 44.33 ± 3.78 s, $P < 0.001$). What's more,
389 the Cre-dependent TRPC6-overexpression in VTA DAT-Cre mice rescued the
390 selective-TRPC6-knockdown-induced depression-like behaviors (**Fig.7E-H**). These
391 results suggest downregulation of TRPC6 in the VTA DA neurons confers the mice
392 with phenotypes of depression/anxiety.
393

394 ## Discussion

395 In this study, we made a systematic study on the molecular mechanism for the
396 subthreshold depolarization that drive spontaneous firing of the VTA DA neurons. We
397 identified TRPC6 channels, alongside NALCN, as major contributors to this
398 subthreshold depolarization and related spontaneous firing, and further importantly,
399 we also demonstrated that TRPC6 contributed to the altered firing activity of the VTA
400 DA neurons under states of depression behaviors.
401 The featured nature of a relatively depolarized resting membrane potential in the VTA
402 DA neurons imposes a need for a full understanding of the channel conductance
403 underlying this depolarization. It is first clear from this current and previous studies
404 that this conductance is mediated by a persistent Na^+ influx. Unlike the DA neurons in
405 the SNc, where Ca^{2+} influx is needed for the spontaneous firing [48], the results in our

406 and others' studies indicate Ca^{2+} influx are not necessary for the spontaneous firing of
407 the VTA DA neurons, rather, replacement of Ca^{2+} ions in the extracellular fluid with
408 Mg^{2+} accelerates the frequency of spontaneous firing (Fig. 1B) [15], possibly due to a
409 reduced activity of the Ca^{2+}-activated K^+ currents. In consistent with these finding and
410 more precisely for a role of Ca^{2+} influx on the subthreshold depolarization, removing
411 extracellular Ca^{2+} did not hyperpolarize the RMP. On the other hand, in consistent the
412 previous study [15], a TTX-insensitive Na^+ influx clearly contributed to the subthreshold
413 depolarization (Fig. 1D).
414 A TTX-insensitive nature of this Na^+ conductance suggests it is likely that cation
415 conductance permeable to Na^+ are the molecular correlates. We first focused on the
416 HCN channels because, (1) it has been suggested HCN channels are important
417 regulators for the spontaneous firing of VTA DA neurons under states of depression
418 behaviors[7, 11]; (2) HCN are among most highly expressed NSCCs in the VTA DA
419 neurons in our single cell RNA-Seq study; (3) HCN are permeable to Na^+ [49]. However,
420 it is clear from our study that HCN does not contribute to the spontaneous firing of the
421 VTA DA neurons in the adult mice; none of the known HCN blockers we used had
422 any significant effects on the firing activity. Presence of HCN has long been used as a
423 signature of DA neurons[50], also as a differentiating factor for the projection-specificity
424 of the VTA DA neurons[38]. Nonetheless, contribution of HCN to the spontaneous firing
425 of the VTA DA neurons has been controversial; the HCN blockers ZD7288 and CsCl
426 have been reported as both effective[23, 24, 51] and non-effective [15] on the spontaneous
427 firing of the VTA DA neurons. A closer inspection into our and others' results present
428 a possible explanation for these different results: in the younger rodents (less than one
429 month old) (sFig. 4) [52], the HCN in the DA neurons play a more important role
430 whereas in the adult mice (~ 8 weeks)[52], like the ones we used in this study, the HCN
431 do not contribute to the spontaneous firing of the VTA DA neurons. This is likely due
432 to a shift of activation gating of HCN channels in a hyperpolarization direction with
433 age, thus the modulation of HCN on the firing activity diminishes with age, as it is
434 described in the SNc DA neurons[52]. In consistent with this, we found hyperpolarizing
435 the RMP rendered the VTA DA neurons of the adult mice with sensitivity to the HCN

436 blockers. Thus, the VTA DA neurons in adult mice do not use HCN to depolarize the
437 membrane to generate action potentials.
438 NALCN is widely expressed in central neurons[53, 54], and is a popular candidate
439 considered for the ion mechanism of the subthreshold depolarization currents and Na^+
440 leaky currents. NALCN has been shown to be an important component of background
441 Na^+ currents and to be important for neuronal excitability in the hippocampal neurons,
442 posterior rhomboid nucleus (Retrotrapezoid nucleus/RTN)) chemo-sensitive neurons
443 (CO_2/H^+-sensitive neurons), GABA neurons and DA neurons in the substantia nigra,
444 spinal projection neurons [26, 28-31, 41]. Our results with single cell RNA-Seq and
445 immunofluorescence methods validated high level expression of NALCN in the VTA
446 DA neurons; both the pharmacological and the NALCN-gene-knockout experiments
447 demonstrated convincingly involvement of NALCN in subthreshold depolarization
448 and spontaneous firing of the VTA DA neurons.
449 We did not detect alteration of NALCN protein expression in the depression model of
450 CMUS in the VTA tissue. However, this does not completely exclude a possible
451 contribution of NALCN to the altered functional activity of the VTA DA neurons
452 which underlies the depression behaviors. Future study focusing on the functional
453 property of NALCN in the cellular level of the VTA DA neurons under a state of
454 depression is needed to clarify this issue. NALCN is after all a potential drug target in
455 consideration of its important contribution to the resting membrane potential and
456 functional activity of neurons.
457 The most interesting and important finding of this study is the role of TRPC6 in
458 regulation of the firing activity of the VTA DA neurons in both physiological and
459 depression-state conditions, and its involvement in depression-like behaviors; the
460 experimental evidence from pharmacological, gene silencing, electrophysiological
461 and behavior results unambiguously support this conclusion. It is interesting to note,
462 although with an unclear neuronal circuit mechanism of action, the TRPC6 channel
463 opener hyperforin was previously reported to have antidepressant effects in
464 corticosterone-depressed mice, which were reversed by prior administration of the
465 TRPC6 blocker larixyl acetate[55]. Also, in a CMUS rat model, TRPC6 expression was

466 found to be downregulated in the hippocampus, and administration of the TRPC6
467 opener hyperforin was effective in alleviating depression-like behavior[56]. Our study
468 provides strong and convincing evidence that TRPC6 is a key regulator of the VTA
469 DA neurons which are known to be a key player in depression states [7, 21, 57-59].
470 The above-mentioned role for TRPC6 should come from its contribution to the
471 subthreshold depolarization, through a persistent permeation to the influx of Na^+.
472 Although TRPC channels has been better recognized for their permeability to Ca^{2+}
473 and their regulation on cellular Ca^{2+} homeostasis, the importance of TRPC channels
474 for the permeability of monovalent cations, especially Na^+, is now gradually being
475 appreciated [60]. In the substantial nigra GABA and DA neurons, TRPC3 has been
476 reported to play an important role in maintaining depolarization membrane potential,
477 pacemaking, and firing regularity[31, 33]. TRPC6 and TRPC3 belong to the same TRPC
478 family subclass and TRPC6 is more than 75% homologous to TRPC3[44]. Interestingly,
479 our results with RNA-Seq and single-cell PCR demonstrated the rich expression of
480 TRPC6 in the VTA DA neurons among all TRP channels but no expression of TRPC3
481 was found in these neurons. These results present an opportunity for selectively
482 targeting a single TRPC channel to exert selective pharmacological results.
483 It has also been demonstrated in cell types other than neurons, such as rat portal vein
484 smooth muscle cells, the activation of α-adrenergic receptor can open TRPC6, which
485 leads to cell depolarization, activation of voltage-dependent Ca^{2+} channels, and
486 ultimately the contraction of smooth muscle cell[61]; it is also shown that angiotensin II
487 and endothelin I can activate TRPC3/C6 heterodimers via vascular G protein-coupled
488 receptors (GPCR), thereby depolarizing cells [62, 63]. Following this line, it would be
489 very interesting to know if TRPC6 in the VTA DA neurons, where multiple GPCR
490 reside receiving input and auto modulation by neuronal transmitters [64, 65], could also
491 be a target of modulation with similar mechanism. In consideration of the important
492 role we described here in this study, this type of modulation will present possible
493 explanations for some unsolved mechanism for physiological and pathophysiological
494 functions of the VTA DA neurons.

495 The facts that downregulation of TRPC6 proteins was correlated with reduced firing
496 activity of the VTA DA neurons, the depression-like behaviors, and that knocking
497 down of TRPC6 in the VTA DA neurons confer the mice with depression behaviors
498 strongly suggest a crucial role for TRPC6 in the development of depression-like
499 behaviors under stressful conditions like CMUS. To reinforce this, downregulation of
500 TRPC6 was also found in another depression model of CRS, a model with similar
501 neuronal alteration of reduced firing activity in the VTA DA neurons to that described
502 in the CMUS model[66]. These facts with the fact that TRPC6 activator hyperforin is an
503 effective antidepressant in multiple depression model[55, 56], and that hyperforin is the
504 principal component of St. John's wort, a well-known antidepressant herb[67], present
505 TRPC6 as very attractive drug target for new lines of antidepressants.

506 **Materials and methods**

507 **Animal Preparation**

508 Male 6-8-week-old C57BL/6 (Vital River, China) and DAT-Cre mice with a C57BL/6
509 background (Stock No: 006660, the Jackson Laboratories, USA) were used for the
510 studies. All experiments were conducted in accordance with the guidelines of Animal
511 Care and Use Committee of Hebei Medical University and approved by the Animal
512 Ethics Committee of Hebei Medical University.

513 **Brain slice preparation**

514 The details for the preparation of coronal brain slice containing VTA were the same as
515 described in our previously published work[21, 64]. Briefly, mice were anesthetized
516 with chloral hydrate (200 mg/kg, i.p.). After intracardial perfusion with ice-cold
517 sucrose solution, the brains of the mice were removed quickly and placed into the
518 slicing solution. The ice-cold sucrose-cutting solution contained (in mM): sucrose 260,
519 $NaHCO_3$ 25, KCl 2.5, NaH_2PO_4 1.25, $CaCl_2$ 2, $MgCl_2$ 2, and D-glucose 10;
520 osmolarity, 295-305 mOsm). Using the vibratome (VT1200S; Leica, Germany), the
521 coronal midbrain slices (250 μm-thick) containing VTA were sectioned. The slices
522 were incubated for 30 min at 36°C in oxygenated artificial cerebrospinal fluid (ACSF)
523 (in mM: NaCl 130, $MgCl_2$ 2, KCl 3, NaH_2PO_4-$2H_2O$ 1.25, $CaCl_2$ 2, D-Glucose 10,
524 $NaHCO_3$ 26; osmolarity, 280-300 mOsm), and were then left for recovery for 60 min

525 at room temperature (23-25°C) until use.

526 The brain slices were transferred to the recording chamber and were continuously
527 perfused with fully oxygenated ASCF during recording.

528 **Identification of DA neurons and electrophysiological recordings**

529 Recordings in the slices were performed in whole-cell current-clamp and
530 voltage-clamp configurations on the Axoclamp 700B preamplifier (Molecular Devices,
531 USA) coupled with a Digidata 1550B AD converter (Molecular Devices, USA).
532 Neurons in the VTA were visualized with a 40X water-immersion objective equipped
533 by an optiMOS microscope camera (Qimaging, Canada) on an Olympus-BX51
534 microscope (Olympus, Japan). Projection-specific or GFP-positive VTA neurons were
535 identified by infrared-differential interference contrast (IR-DIC) video microscopy
536 and epifluorescence (Olympus, Japan) for detection of retrobeads (red) positive or
537 GFP-positive neurons.

538 For whole-cell recording, glass electrodes (3-5 MΩ) were filled with internal solution
539 (in mM): K-methylsulfate 115, KCl 20, $MgCl_2$ 1, HEPES 10, EGTA 0.1, MgATP 2
540 and Na_2GTP 0.3, pH adjusted to 7.4 with KOH. And the extracellular solution was the
541 ACSF.

542 In whole-cell current-clamp mode, HCN function was judged by the inwardly
543 rectifying characteristic sag potential generated by giving a hyperpolarizing current
544 (-100 pA).

545 When recording the effect of removing extracellular Ca^{2+} on spontaneous cell
546 discharge, $CaCl_2$ in the ACSF was replaced with $MgCl_2$, and the final $MgCl_2$
547 concentration was 4 mM.

548 The resting membrane potential (RMP) was measured in current clamp mode (I = 0);
549 the composition of the recording solution (mM) contained: NaCl 151, KCl 3.5, $CaCl_2$
550 2, $MgCl_2$ 1, glucose 10, and HEPES 10, and the pH was adjusted to about 7.35 with
551 NaOH. 1 μM tetrodotoxin was added to the extracellular solution to abolish action
552 potential during measurement of the RMP.

553 To observe the effect of extracellular Na^+ on the RMP, NaCl in the original recording
554 solution was replaced with equimolar NMDG, and the NMDG-recording solution
555 (mM) contained: NMDG 151, KCl 3.5, $CaCl_2$ 2, $MgCl_2$ 1, glucose 10, and HEPES 10,

556 and the pH was adjusted to 7.35 with KOH.
557 For recording spontaneous firing of the neurons, cell-attached "loose-patch" (100-300
558 MΩ) recordings were used[68]. In this case, patch-pipettes (2-4 MΩ) were filled with
559 ACSF, and the spontaneous activity was recorded in the current-clamp mode (I = 0).
560 The synaptic blockers (CNQX, 10 μM; APV, 50 μM and gabazine, 10 μM) were
561 added to isolate the intrinsic firing properties.
562 At the end of electrophysiological recordings, the recorded VTA neurons were
563 collected for single-cell PCR. VTA DA neurons were identified by single-cell PCR for
564 the presence of TH and DAT.
565
566 **Retrograde labelling**
567 Briefly, under general chloral hydrate anaesthesia (200 mg/kg, i.p.) and stereotactic
568 control (RWD Instruments, Guangzhou, China), the skull surface was exposed. All
569 coordinates are relative to bregma in mm using landmarks and neuroanatomical
570 nomenclature that was described in the Franklin and Paxinos mouse brain atlas[69] . Red
571 retrobeads (100 nl for single injection; Lumafluor Inc., Naples, FL, USA) were
572 injected into the following sites using KD scientific syringe pump (KD scientific,
573 Holliston MA, USA): bilaterally into NAc core (NAc c), NAc lateral shell (NAc ls),
574 NAc medial shell (NAc ms) and basolateral amygdala (BLA), 4 separate sites (2 per
575 hemisphere) into medial prefrontal cortex (mPFC). Coordinates for infusions were as
576 follows: NAc c (AP +1.50, LM 0.84, DV -4.0; 100 nl beads); NAc ls (AP +0.86, LM
577 1.72, DV -4.0; 100 nl beads); NAc ms (AP +1.70, LM 0.53, DV -4.0; 100 nl beads);
578 mPFC (AP +2.05 and 2.15, LM 0.27, DV -2.1 + 1.7; 200 nl beads); BLA (AP -1.46,
579 LM 2.85, DV -4.3; 100 nL beads). Retrobeads were delivered through a pulled glass
580 pipette using a PAP107 Multipipette Puller (MicroData Instrument, Inc., USA) and at
581 a rate of 100 nl/min; the injection needle was left in place for at least 5 minutes after
582 each infusion. Following surgery, mice were returned to single housing. For sufficient
583 labelling, survival periods for retrograde tracer transport depended on respective
584 injection areas: NAc c, NAc ls, NAc ms, 14 days; mPFC, 21 days; BLA 14 days.
585 Coronal sections of injection sites were stained with 4, 6-diamidino-2-phenylindole
586 (DAPI, Sigma, USA) to confirm representative target location. Then, serial analyses

587 of the injection-sites were carried out routinely.

588

589 **AAV for gene knockdown or overexpression and viral construct and injection**

590 For knockdown of NALCN and TRPC6, AAV9-U6-shRNA (NALCN)-CMV-GFP
591 (300 nl) or AAV9-U6-shRNA (TRPC6)-CMV-GFP or its control
592 AAV9-scramble-shRNA was delivered into the VTA (AP, −3.08 mm; ML, ±0.50 mm;
593 DV, −4. 50 mm) of the mice. AAV9-hSyn-DIO-shRNA (TRPC6)-RFP (300 nl) or its
594 control AAV9-scramble-shRNA was delivered into the VTA of the DAT-Cre C57BL/6
595 mice.

596 The shRNA hairpin sequences used in this study: NALCN shRNA:
597 AAGATCGCACAGCCTCTTCAT[26]; TRPC6 shRNA: 5'-
598 CCAGGATCAATGCATACAA-3'.

599 For Cre-dependent overexpression of TRPC6, AAV9-DIO-TRPC6-GFP (300 nl) or its
600 control AAV9-scramble-RNA was delivered into the VTA of the DAT-Cre C57BL/6
601 mice.

602 **Single cell PCR**

603 mRNA was reversely transcribed to cDNA by PrimeScript™II1st Strand cDNA
604 Synthesis Kit (Takara-Clontech, Kyoto, Japan). At the end of electrophysiological
605 recordings, the recorded neuron was aspirated into a pipette and then expelled into a
606 PCR sterile tube containing 1 μl oligo-dT Primer and 1 μl dNTP mixture. The mixture
607 was heated to 65°C for 5 min to denature the nucleic acids and then cooled on ice for
608 2 min. Reverse transcription from mRNA into cDNA was performed at 50°C for 50
609 min and then 85°C for 5 sec. cDNA was stored at -40°C. Then two rounds of
610 conventional PCR with pairs of gene-specific outside (first round) and inner primers
611 (second round) for GAPDH (positive control), TH, DAT, D2, GIRK2, Vgult2, GAD1,
612 NALCN, TRPC6, TRPV2 and TRPC3 using GoTaq Green Master Mix (Promega,
613 Madison, USA) were performed. After adding the specific outside primer pairs into
614 each PCR tube, first-round synthesis conditions were as follows: 95 °C (5 min); 30
615 cycles of 95 °C (50 s), 58-62 °C (50 s), 72 °C (50 s); 72 °C (5 min). Then, the product
616 of the first PCR was added in the second amplification round by using specific inner
617 primer (final volume 25 μl). The second amplification round consisted of the

618 following: 95 °C (5 min); 35 cycles of 95 °C (50 s), 58 °C-62 °C (45 s), 72 °C (50 s)
619 and 5 min elongation at 72 °C. The final PCR products were separated by
620 electrophoresis on 2% agarose gels. The negative control reactions with no added
621 template were also performed in each experiment.
622 The "outer" primers (from 5′ to 3′) as follows:
623 GAPDH:
624 AAATGGTGAAGGTCGGTGTGAACG（sense）
625 AGTGATGGCATGGACTGTGGTCAT （antisense）
626 TH:
627 GCCGTCTCAGAGCAGGATAC
628 GGGTAGCATAGAGGCCCTTC
629 DAT:
630 CTGCCCTGTCCTGAAAGGTGT
631 GCCCAGTGATCACAGACTCC
632 D2-R:
633 AGCATCGACAGGTACACAGC
634 CCATTCTCCGCCTGTTCACT
635 GIRK2:
636 TGGACCAGGATGTGGAAAGC
637 AAACCCGTTGAGGTTGGTGA
638 Vgult2:
639 CTGCTTCTGGTTGTTGGCTACTCT
640 ATCTCGGTCCTTATAGGTGTACGC
641 GAD1:
642 ACAACCTTTGGCTGCATGTGGATG
643 AATCCCACGGTGCCCTTTGCTTTC
644 NALCN:
645 TCCATCTGTGGGAAGCATGT
646 CAAAAGCTGGTCCTCTTCAGTG
647 TRPC6:
648 AGCCTGTCTATTGAGGAAGAAC

AGCGAGAATGATTGGGGTCA

TRPV2:

CTGCACATCGCCATAGAGAA

AGGCTGGTGGTAGGCAACTA

TRPC3:

GCTGGCCAACATAGAGAAGG

CCTGCACGTGACTATCCACA

The “inner” primers (from 5′ to 3′) as follows:

GAPDH:

GCAAATTCAACGGCACAGTCAAGG

TCTCGTGGTTCACACCCATCACAA

TH:

AGGAGAGGGATGGAAATGCT

ACCAGGGAACCTTGTCCTCT

DAT:

ATTTTGAGCGTGGTGTGCTG

TGCCTCACAGAGACGGTAGA

D2-R:

CCATTGTCTGGGTCCTGTCC

GTGGGTACAGTTGCCCTTGA

GIRK2:

AGCCGAGACAGGACCAAAAG

ATGTACGCAATCAGCCACCA

Vgult2:

CATCTCCTTCTTGGTGCTTGCAGT

ACAGCGTGCCAACGCCATTTGAAA

GAD1:

AGTCACCTGGAACCCTC

GCTTGTCTGGCTGGAA

NALCN:

GCCTTTGCTGGAGTTGTTCTG

680 CCCTGCATAATTGCCACAGTC
681 TRPC6:
682 TGCTAGAAGAGTGTCATTCCCT
683 CCTCCACAATCCGTACATAACC
684 TRPV2:
685 GTGGGATGTGGTGACCTACC
686 GCTGGTACAGCCCTGAGAAC
687 TRPC3:
688 CCTTGGGTCTTCCATTCCTC
689 CACAACTGCACGATGTACTCC
690
691 **RT-qPCR**
692 Total RNA was prepared using Trizol. RNA was reversely transcribed into cDNA by
693 TAKARA PrimeScripttm RT reagent Kit with gDNA Eraser for Reverse transcription.
694 Subsequently, the SYBR Green Master Mix (TaKaRa) was used to do the qRT-PCR
695 assays.
696 The specific primers were:
697 GAPDH：
698 GCAAATTCAACGGCACAGTCAAGG
699 TCTCGTGGTTCACACCCATCACAA
700 TRPC6：
701 GCAGAAACACAGAGGAAGTGG
702 GCTCTTTCCAGCTTGGCATATC
703 NALCN：
704 TAATGAGATAGGCACGAGTA
705 TGATGAAGTAGAAGTAGGAG
706
707 **Single cell RT-qPCR**
708 Following the retrograde labelling and VTA brain slice preparation,
709 projection-specific VTA neurons were identified by infrared-differential interference
710 contrast (IR-DIC) video microscopy and epifluorescence (Olympus, Japan) for

711 detection of retrobeads (red) positive neurons. mRNA was reversely transcribed to
712 cDNA by PrimeScript^{TM}II1st Strand cDNA Synthesis Kit (Takara-Clontech, Kyoto,
713 Japan). The projection-specific neurons was aspirated into a pipette and then expelled
714 into a PCR sterile tube containing 1 μl oligo-dT Primer and 1 μl dNTP mixture. The
715 mixture was heated to 65°C for 5 min to denature the nucleic acids and then cooled on
716 ice for 2 min. Reverse transcription from mRNA into cDNA was performed at 50°C
717 for 50 min and then 85°C for 5 sec. cDNA was stored at -40°C. The targeted
718 pre-amplification was done, with pairs of targeted primers for GAPDH, TH and
719 TRPC6, to quantify multiple targets per cell. After adding the targeted primer pairs
720 into each PCR tube, the synthesis conditions were as follows: 95 °C (5 min); 10
721 cycles of 95 °C (50 s), 58-62 °C (50 s), 72 °C (50 s); 72 °C (5 min). After targeted
722 pre-amplification, Quantitative PCR (qPCR) is the final laboratory step of the
723 scRT-qPCR workflow with the SYBR Green Master Mix (TaKaRa).
724 The targeted primers for pre-amplification (from 5′ to 3′) as follows:
725 GAPDH:
726 AAATGGTGAAGGTCGGTGTGAACG（sense）
727 AGTGATGGCATGGACTGTGGTCAT （antisense）
728 TH:
729 AAGGTTCATTGGACGGCGG
730 ACATCGTCAGACACCCGAC
731 TRPC6:
732 AGCCTGTCTATTGAGGAAGAAC
733 AGCGAGAATGATTGGGGTCA
734 The primers for qPCR (from 5′ to 3′) as follows:
735 GAPDH:
736 GCAAATTCAACGGCACAGTCAAGG
737 TCTCGTGGTTCACACCCATCACAA
738 TH:
739 TCTCCTTGAGGGGTACAAAACC
740 ACCTCGAAGCGCACAAAGT
741 TRPC6:

742 TGCTAGAAGAGTGTCATTCCCT
743 CCTCCACAATCCGTACATAACC
744
745 **Immunofluorescence**
746 After intracardial perfusion with 4% paraformaldehyde (PFA) in 0.01 M PBS (pH 7.4).
747 The brains were post-fixed in 4% paraformaldehyde. 48 h later, the brain tissue was
748 placed in 30% sucrose solution (PBS preparation) to dehydrate. The brain tissue was
749 sectioned coronally, including the nucleus accumben (NAc), medial prefrontal cortex
750 (mPFC), basolateral amygdala (BLA), and VTA, using a vibrating microtome. The
751 section thickness was 40 μm. The sections were placed in PBS solution and stored in
752 a refrigerator at 4°C for storage.
753 The brain section was incubated in 0.3% triton/3% BSA for 1 h at room temperature
754 and then was blocked with 10% donkey serum at 37℃ for 1 h. After that, the brain
755 section was incubated in the corresponding antibodies in PBS at 4℃ for 24 h. The
756 section was washed three times (10 min) with PBS. Finally, the brain section was
757 incubated in the secondary antibodies for 2 h at 37℃. Images were obtained on a
758 Leica TCS SP5 confocal laser microscope (Leica, Germany) equipped with laser lines
759 for 405 mm, 488 mm, 561 mm and 647 mm illumination. Images were analyzed with
760 LAS-AF-Lite software (Leica, Germany).
761
762 **Single-cell whole-transcriptome gene sequencing**
763 After retrobeads injection, following brain slice preparation and 1 h recording, the
764 recorded and retrobeads-labeled neurons were aspirated into the patch pipette and
765 were then broken into the PCR tube containing 1 μl lysis buffer. For mRNA in
766 individual cells, mRNA was amplified and cDNA by SMARTer Ultra Low Input RNA
767 for Illumina Kit, which was qualified and reversely transcribed to cDNA by Qubit and
768 Agilent Bioanalyzer 2100 electrophoresis. After fragmentation of cDNA (300 bp) by
769 ultrasound, sequencing libraries (end repair, addition of poly(A), and ligation of
770 sequencing connectors) were built using the Ovation Ultralow Library System V2.
771 After that, the constructed libraries were sequenced using Illumina HiseqXten
772 (Sinotech Genomics Co., Ltd.).

773

774 **Depression models**

775 Chronic Mild Unpredictable Stress (CMUS) procedure

776 The CMUS procedures consisted of food and water deprivation (24 h), day/night
777 inversion, damp bedding (12 h), cage tilt (12 h), no bedding (12 h), rat bedding (12 h),
778 4°C cold bath (5 min), restraint (2 h) and tail pinching (30 min). mice were subjected
779 to consecutive 35 days of CMUS with two stressors per day. Non-stressed controls
780 were handled only for cage changes and behavioral tests.

781 Chronic Restraint Stress (CRS) procedure

782 The mice were immobilized in a special restraint device for 6 h per day from 9:00 to
783 15:00 for 21 days.

784 Behavior tests

785 Sucrose preference test

786 Mice were single-housed and trained to drink from two drinking bottles with 1 bottle
787 of tap water and 1 bottle of 1% sucrose water, for 48 hours, and the positions of the
788 drinking bottles were exchanged every 12 h to exclude the interference of position
789 preference. After the training, the mice were deprived of food and water for 12 h, and
790 then the sucrose preference test was performed for 24 h. One bottle of tap water and
791 one bottle of 1.0 % sucrose water were given again, and the positions of the drinking
792 bottles were exchanged at 12 h. Finally, the consumption of tap water and sugar water
793 at 24 h were recorded to calculate the sucrose solution preference rate. Sucrose
794 preference rate = sucrose solution consumption/(tap water consumption + sucrose
795 solution consumption).

796 Tail suspension test, TST

797 Mouse was suspended by taping the tail (1 cm from the tip of the tail) to the fixation
798 device for 6 min. The cumulative immobility time within last 4 min was recorded, and
799 the time when all limbs were immobile except for respiration was considered as
800 immobility time.

801 Forced swimming test, FST

802 Forced swimming test (FST) was performed in a glass cylinders, filled with the water
803 depth about 10 cm at room temperature. The experiment was conducted for 5 min, of

804 which the first 1 min was the adaptation time and the mice were allowed to move
805 freely, and the immobility time was recorded for last 4 min after the adaptation.
806 Open field test, OFT
807 The mice were placed in a topless chamber (40 cm × 40 cm × 30 cm) with a camera
808 mounted on top of the chamber and connected to ANY-maze video tracking system on
809 the computer to automatically track and record the activity of mice during the
810 experiment and to obtain behavioral data. The bottom of the chamber was divided into
811 16 small square grids (10 cm × 10 cm) on the computer, and four square grids in the
812 central area were defined as the central zone. During the 10 min test session, Total
813 distance traveled and time spent in the center were recorded.
814 Elevated plus maze, EPM
815 The EPM apparatus consists of two closed arms (25 x 5 cm) across from each other
816 and perpendicular to two open arms (25 x 5 cm) that are connected by a center
817 platform (5 x 5 cm), with a camera in the center ceiling to automatically track and
818 record the activity of mice. Mice were placed in the center platform facing a closed
819 arm and allowed to freely explore the maze for 7 min, of which the first 2 min was the
820 adaptation time. The time spent in open arms was analyzed for last 5 min after the
821 adaptation.
822
823 **Western Blot**
824 The VTA protein was isolated by100 μl RIPA and 1 μl PMSF. The total protein for
825 each sample was transferred onto the polyvinylidene difluoride (PVDF) membranes
826 after SDS-polyacrylamide gel electrophoresis (SDS-PAGE), and blocked 2 h at room
827 temperature with 5% bovine serum albumin (KeyGen Biotechnology). Subsequently,
828 all these membranes were incubated overnight at 4 °C with the primary antibodies as
829 below: TRPC6, NALCN, and GAPDH. Following 2 h secondary antibodies
830 incubation, all the bands were detected. The relative expression was calculated based
831 on the internal control GAPDH.
832
833 **Drugs and reagents**
834 Drugs were bath applied at the following concentrations:

835 6-cyano-7-nitroquinoxaline-2,3-dione (CNQX; 10 μM; Sigma),
836 DL-2-amino-5-phosphonopentanoic acid (APV; 50 μM; Sigma) and gabazine (10 μM;
837 Sigma), CsCl (3mM; sigma), ZD7288(60 μm; Abcam), TTX (1 μM; MCE), $GdCl_3$
838 (100 μM; Sigma), 2-Aminoethyldiphenylborinate (2-APB, 100 μM; Sigma),
839 Flufenamic acid (100 μM; alomone), Ruthenium Red (60 μM; TCI).
840 Commercial antibodies used were: Anti-Tyrosine Hydroxylase Antibody (1:400,
841 Millipore, MAB318, RRID:AB_2201528, for Immunofluorescence), Anti-Dopamine
842 Transporter (N-terminal) antibody (1:400, sigma, D6944, RRID:AB_1840807, for
843 Immunofluorescence), Anti-NALCN (1:100, Thermo Fisher Scientific, MA5-27593,
844 RRID:AB_2735285, for Immunofluorescence), Anti-TRPC6 (1:100, Alomone,
845 ACC-017, RRID:AB_2040243, for Immunofluorescence), Anti-GAPDH (1:10000,
846 Santa Cruz, sc-137179, RRID:AB_2232048, for Western Blot), Anti-NALCN (1:100,
847 GeneTex, GTX54808, for Western Blot), Anti-TRPC6 (1:100, Cell Signaling
848 Technology, 16716, RRID:AB_2798768, for Western Blot).
849 Secondary antibodies: Donkey anti-Mouse IgG (H+L) Highly Cross-Adsorbed
850 Secondary Antibody (Alexa Fluor 488, Thermo Fisher Scientific, A-21202, 1:1000),
851 Donkey anti-Mouse IgG (H+L) Highly Cross-Adsorbed Secondary Antibody (Alexa
852 Fluor 546, Thermo Fisher Scientific, A10037, 1:1000), Donkey anti-Rabbit IgG (H+L)
853 Highly Cross-Adsorbed Secondary Antibody (Alexa Fluor 488, Thermo Fisher
854 Scientific, A21206, 1:1000), Donkey anti- Rabbit IgG (H+L) Highly Cross-Adsorbed
855 Secondary Antibody (Alexa Fluor 546, Thermo Fisher Scientific, A10040, 1:1000),
856 Donkey anti- Rabbit IgG (H+L) Highly Cross-Adsorbed Secondary Antibody (Alexa
857 Fluor 647, Thermo Fisher Scientific, A31573, 1:1000)
858
859 **Quantification and statistical analysis**
860 Software such as GraphPad Prism6, OriginPro 8.0 (Origin Lab) and Adobe Illustrator
861 CS6 were used for data analysis and image processing. All experimental data were
862 expressed as mean ± standard error (mean ± S.E.M.). When the data were normally
863 distributed, the difference between two groups was statistically analyzed by
864 two-sample T-test or paired-sample T-test; when the data were not normally
865 distributed, the difference between two groups was statistically analyzed by
866 Mann-Whitney U test or Wilcoxon matched-pairs signed rank test. $P < 0.05$ was
867 considered as a statistically significant difference between two groups. For the data

between multiple groups, when the data were normally distributed and there was no significant variance inhomogeneity, one-way ANOVA with Dunnett's multiple comparisons test was used; when the data were not normally distributed, Kruslal-Wallis-H test with Dunnett's multiple comparisons test and Student-Newman-Keuls test with Dunnett's multiple comparisons test were used.

Conflict of Interest

The authors declare that the research was conducted in the absence of any commercial or financial relationships that could be construed as a potential conflict of interest.

Author Contributions

Hailin Zhang conceived, designed and supervised the experiments; Jing Wang performed the experiments, acquired and analyzed the data and prepared the figures; Dongmei Zhang and Min Su performed immunofluorescence of the brain slices and performed some preliminary electrophysiological experiments; Yuqi Sang and Chaoyi Li performed part of single-cell PCR; Yongxue Zhang performed part of statistical analysis; Ludi Zhang and Chenxu Niu took care of mice; Hailin Zhang and Jing Wang wrote the manuscript; Hailin Zhang and Xiaona Du prepared the final version of the manuscript.

Funding

This work was supported by the National Natural Science Foundation of China (81871075, 82071533) grants to HZ; National Natural Science Foundation of China (81870872) grants to XD; Science Fund for Creative Research Groups of Natural Science Foundation of Hebei Province (no. H2020206474); Basic Research Fund for Provincial Universities (JCYJ2021010); Science-Technology Research Foundation of the Higher Education Institutions of Hebei (Z2017073) and Scientific research project of Hebei administration of traditional Chinese Medicine (2017021) grants to WJ.

Acknowledgments

We would like to thank Dr. Lili for the technical assistance.

Data Availability Statement

The data that support the findings of this study are available from the corresponding author upon reasonable request.

References

1. Bromberg-Martin ES, Matsumoto M, Hikosaka O. Dopamine in motivational control: rewarding, aversive, and alerting. *Neuron* 2010; **68**(5)**:** 815-834.
2. Lammel S, Lim BK, Malenka RC. Reward and aversion in a heterogeneous midbrain dopamine system. *Neuropharmacology* 2014; **76 Pt B**(0 0)**:** 351-359.
3. Van den Heuvel DM, Pasterkamp RJ. Getting connected in the dopamine system. *Prog Neurobiol* 2008; **85**(1)**:** 75-93.
4. Chaudhury D, Walsh JJ, Friedman AK, Juarez B, Ku SM, Koo JW *et al.* Rapid regulation of depression-related behaviours by control of midbrain dopamine neurons. *Nature* 2013; **493**(7433)**:** 532-536.
5. Kabanova A, Pabst M, Lorkowski M, Braganza O, Boehlen A, Nikbakht N *et al.* Function and developmental origin of a mesocortical inhibitory circuit. *Nat Neurosci* 2015; **18**(6)**:** 872-882.
6. Badrinarayan A, Wescott SA, Vander Weele CM, Saunders BT, Couturier BE, Maren S *et al.* Aversive stimuli differentially modulate real-time dopamine transmission dynamics within the nucleus accumbens core and shell. *J Neurosci* 2012; **32**(45)**:** 15779-15790.
7. Friedman AK, Walsh JJ, Juarez B, Ku SM, Chaudhury D, Wang J *et al.* Enhancing depression mechanisms in midbrain dopamine neurons achieves homeostatic resilience. *Science* 2014; **344**(6181)**:** 313-319.
8. Krishnan V, Han MH, Graham DL, Berton O, Renthal W, Russo SJ *et al.* Molecular adaptations underlying susceptibility and resistance to social defeat in brain reward regions. *Cell* 2007; **131**(2)**:** 391-404.
9. Grace AA, Floresco SB, Goto Y, Lodge DJ. Regulation of firing of dopaminergic neurons and control of goal-directed behaviors. *Trends Neurosci* 2007; **30**(5)**:** 220-227.
10. Johnson SW, North RA. Two types of neurone in the rat ventral tegmental area and their synaptic inputs. *J Physiol* 1992; **450:** 455-468.
11. Zhong P, Vickstrom CR, Liu X, Hu Y, Yu L, Yu HG *et al.* HCN2 channels in the ventral tegmental area regulate behavioral responses to chronic stress. *Elife* 2018; **7**.
12. Bean BP. The action potential in mammalian central neurons. *Nat Rev Neurosci* 2007; **8**(6)**:** 451-465.
13. Guzman JN, Sánchez-Padilla J, Chan CS, Surmeier DJ. Robust pacemaking in substantia nigra dopaminergic neurons. *J Neurosci* 2009; **29**(35)**:** 11011-11019.
14. Puopolo M, Raviola E, Bean BP. Roles of subthreshold calcium current and sodium current in spontaneous firing of mouse midbrain dopamine neurons. *J Neurosci* 2007; **27**(3)**:** 645-656.
15. Khaliq ZM, Bean BP. Pacemaking in dopaminergic ventral tegmental area neurons: depolarizing drive from background and voltage-dependent sodium conductances. *J Neurosci* 2010; **30**(21)**:** 7401-7413.
16. Beckstead MJ, Grandy DK, Wickman K, Williams JT. Vesicular dopamine release elicits an inhibitory postsynaptic current in midbrain dopamine neurons. *Neuron* 2004; **42**(6)**:** 939-946.
17. Ford CP, Beckstead MJ, Williams JT. Kappa opioid inhibition of somatodendritic dopamine inhibitory postsynaptic currents. *J Neurophysiol* 2007; **97**(1)**:** 883-891.
18. Philippart F, Destreel G, Merino-Sepúlveda P, Henny P, Engel D, Seutin V. Differential Somatic Ca2+ Channel Profile in Midbrain Dopaminergic Neurons. *J Neurosci* 2016; **36**(27)**:** 7234-7245.
19. Dufour MA, Woodhouse A, Goaillard JM. Somatodendritic ion channel expression in substantia nigra pars compacta dopaminergic neurons across postnatal development. *J*

943 *Neurosci Res* 2014; **92**(8)**:** 981-999.
944 20. Kimm T, Khaliq ZM, Bean BP. Differential Regulation of Action Potential Shape and
945 Burst-Frequency Firing by BK and Kv2 Channels in Substantia Nigra Dopaminergic Neurons. *J*
946 *Neurosci* 2015; **35**(50)**:** 16404-16417.
947 21. Li L, Sun H, Ding J, Niu C, Su M, Zhang L *et al.* Selective targeting of M-type potassium K(v) 7.4
948 channels demonstrates their key role in the regulation of dopaminergic neuronal excitability
949 and depression-like behaviour. *Br J Pharmacol* 2017; **174**(23)**:** 4277-4294.
950 22. Tarfa RA, Evans RC, Khaliq ZM. Enhanced Sensitivity to Hyperpolarizing Inhibition in
951 Mesoaccumbal Relative to Nigrostriatal Dopamine Neuron Subpopulations. *J Neurosci* 2017;
952 **37**(12)**:** 3311-3330.
953 23. Seutin V, Massotte L, Renette MF, Dresse A. Evidence for a modulatory role of Ih on the firing
954 of a subgroup of midbrain dopamine neurons. *Neuroreport* 2001; **12**(2)**:** 255-258.
955 24. Neuhoff H, Neu A, Liss B, Roeper J. I(h) channels contribute to the different functional
956 properties of identified dopaminergic subpopulations in the midbrain. *J Neurosci* 2002; **22**(4)**:**
957 1290-1302.
958 25. Krashia P, Martini A, Nobili A, Aversa D, D'Amelio M, Berretta N *et al.* On the properties of
959 identified dopaminergic neurons in the mouse substantia nigra and ventral tegmental area.
960 *Eur J Neurosci* 2017; **45**(1)**:** 92-105.
961 26. Shi Y, Abe C, Holloway BB, Shu S, Kumar NN, Weaver JL *et al.* Nalcn Is a "Leak" Sodium
962 Channel That Regulates Excitability of Brainstem Chemosensory Neurons and Breathing. *J*
963 *Neurosci* 2016; **36**(31)**:** 8174-8187.
964 27. Lu B, Su Y, Das S, Wang H, Wang Y, Liu J *et al.* Peptide neurotransmitters activate a cation
965 channel complex of NALCN and UNC-80. *Nature* 2009; **457**(7230)**:** 741-744.
966 28. Philippart F, Khaliq ZM. G(i/o) protein-coupled receptors in dopamine neurons inhibit the
967 sodium leak channel NALCN. *Elife* 2018; **7**.
968 29. Lutas A, Lahmann C, Soumillon M, Yellen G. The leak channel NALCN controls tonic firing and
969 glycolytic sensitivity of substantia nigra pars reticulata neurons. *Elife* 2016; **5**.
970 30. Ford NC, Ren D, Baccei ML. NALCN channels enhance the intrinsic excitability of spinal
971 projection neurons. *Pain* 2018; **159**(9)**:** 1719-1730.
972 31. Um KB, Hahn S, Kim SW, Lee YJ, Birnbaumer L, Kim HJ *et al.* TRPC3 and NALCN channels drive
973 pacemaking in substantia nigra dopaminergic neurons. *Elife* 2021; **10**.
974 32. Kim SH, Choi YM, Jang JY, Chung S, Kang YK, Park MK. Nonselective cation channels are
975 essential for maintaining intracellular Ca2+ levels and spontaneous firing activity in the
976 midbrain dopamine neurons. *Pflugers Arch* 2007; **455**(2)**:** 309-321.
977 33. Zhou FW, Matta SG, Zhou FM. Constitutively active TRPC3 channels regulate basal ganglia
978 output neurons. *J Neurosci* 2008; **28**(2)**:** 473-482.
979 34. Hof T, Chaigne S, Récalde A, Sallé L, Brette F, Guinamard R. Transient receptor potential
980 channels in cardiac health and disease. *Nat Rev Cardiol* 2019; **16**(6)**:** 344-360.
981 35. German DC, Manaye KF. Midbrain dopaminergic neurons (nuclei A8, A9, and A10):
982 three-dimensional reconstruction in the rat. *J Comp Neurol* 1993; **331**(3)**:** 297-309.
983 36. Nair-Roberts RG, Chatelain-Badie SD, Benson E, White-Cooper H, Bolam JP, Ungless MA.
984 Stereological estimates of dopaminergic, GABAergic and glutamatergic neurons in the ventral
985 tegmental area, substantia nigra and retrorubral field in the rat. *Neuroscience* 2008; **152**(4)**:**
986 1024-1031.

987 37. Cadwell CR, Palasantza A, Jiang X, Berens P, Deng Q, Yilmaz M *et al.* Electrophysiological,
988 transcriptomic and morphologic profiling of single neurons using Patch-seq. *Nat Biotechnol*
989 2016; **34**(2)**:** 199-203.
990 38. Lammel S, Hetzel A, Häckel O, Jones I, Liss B, Roeper J. Unique properties of mesoprefrontal
991 neurons within a dual mesocorticolimbic dopamine system. *Neuron* 2008; **57**(5)**:** 760-773.
992 39. Kawano M, Kawasaki A, Sakata-Haga H, Fukui Y, Kawano H, Nogami H *et al.* Particular
993 subpopulations of midbrain and hypothalamic dopamine neurons express vesicular
994 glutamate transporter 2 in the rat brain. *J Comp Neurol* 2006; **498**(5)**:** 581-592.
995 40. Stamatakis AM, Jennings JH, Ung RL, Blair GA, Weinberg RJ, Neve RL *et al.* A unique
996 population of ventral tegmental area neurons inhibits the lateral habenula to promote
997 reward. *Neuron* 2013; **80**(4)**:** 1039-1053.
998 41. Lu B, Su Y, Das S, Liu J, Xia J, Ren D. The neuronal channel NALCN contributes resting sodium
999 permeability and is required for normal respiratory rhythm. *Cell* 2007; **129**(2)**:** 371-383.
1000 42. Kusch J, Biskup C, Thon S, Schulz E, Nache V, Zimmer T *et al.* Interdependence of receptor
1001 activation and ligand binding in HCN2 pacemaker channels. *Neuron* 2010; **67**(1)**:** 75-85.
1002 43. Mistrík P, Mader R, Michalakis S, Weidinger M, Pfeifer A, Biel M. The murine HCN3 gene
1003 encodes a hyperpolarization-activated cation channel with slow kinetics and unique response
1004 to cyclic nucleotides. *J Biol Chem* 2005; **280**(29)**:** 27056-27061.
1005 44. Clapham DE, Runnels LW, Strübing C. The TRP ion channel family. *Nat Rev Neurosci* 2001; **2**(6)**:**
1006 387-396.
1007 45. Willner P. The chronic mild stress (CMS) model of depression: History, evaluation and usage.
1008 *Neurobiol Stress* 2017; **6:** 78-93.
1009 46. Liu D, Tang QQ, Yin C, Song Y, Liu Y, Yang JX *et al.* Brain-derived neurotrophic factor-mediated
1010 projection-specific regulation of depressive-like and nociceptive behaviors in the mesolimbic
1011 reward circuitry. *Pain* 2018; **159**(1)**:** 175.
1012 47. Moreines JL, Owrutsky ZL, Grace AA. Involvement of Infralimbic Prefrontal Cortex but not
1013 Lateral Habenula in Dopamine Attenuation After Chronic Mild Stress.
1014 *Neuropsychopharmacology* 2017; **42**(4)**:** 904-913.
1015 48. Kang Y, Kitai ST. A whole cell patch-clamp study on the pacemaker potential in dopaminergic
1016 neurons of rat substantia nigra compacta. *Neurosci Res* 1993; **18**(3)**:** 209-221.
1017 49. Benarroch EE. HCN channels: function and clinical implications. *Neurology* 2013; **80**(3)**:**
1018 304-310.
1019
1020 50. Mercuri NB, Bonci A, Calabresi P, Stefani A, Bernardi G. Properties of the
1021 hyperpolarization-activated cation current Ih in rat midbrain dopaminergic neurons. *Eur J*
1022 *Neurosci* 1995; **7**(3)**:** 462-469.
1023 51. Okamoto T, Harnett MT, Morikawa H. Hyperpolarization-activated cation current (Ih) is an
1024 ethanol target in midbrain dopamine neurons of mice. *J Neurophysiol* 2006; **95**(2)**:** 619-626.
1025 52. Chan CS, Guzman JN, Ilijic E, Mercer JN, Rick C, Tkatch T *et al.* 'Rejuvenation' protects neurons
1026 in mouse models of Parkinson's disease. *Nature* 2007; **447**(7148)**:** 1081-1086.
1027 53. Lee JH, Cribbs LL, Perez-Reyes E. Cloning of a novel four repeat protein related to
1028 voltage-gated sodium and calcium channels. *FEBS Lett* 1999; **445**(2-3)**:** 231-236.
1029 54. Lu TZ, Feng ZP. NALCN: a regulator of pacemaker activity. *Mol Neurobiol* 2012; **45**(3)**:**
1030 415-423.

1031 55. Pochwat B, Szewczyk B, Kotarska K, Rafało-Ulińska A, Siwiec M, Sowa JE *et al.* Hyperforin
1032 Potentiates Antidepressant-Like Activity of Lanicemine in Mice. *Front Mol Neurosci* 2018; **11:**
1033 456.
1034 56. Liu Y, Liu C, Qin X, Zhu M, Yang Z. The change of spatial cognition ability in depression rat
1035 model and the possible association with down-regulated protein expression of TRPC6. *Behav*
1036 *Brain Res* 2015; **294:** 186-193.
1037 57. Tye KM, Mirzabekov JJ, Warden MR, Ferenczi EA, Tsai HC, Finkelstein J *et al.* Dopamine
1038 neurons modulate neural encoding and expression of depression-related behaviour. *Nature*
1039 2013; **493**(7433)**:** 537-541.
1040 58. Chang CH, Grace AA. Amygdala-ventral pallidum pathway decreases dopamine activity after
1041 chronic mild stress in rats. *Biol Psychiatry* 2014; **76**(3)**:** 223-230.
1042 59. Cao JL, Covington HE, 3rd, Friedman AK, Wilkinson MB, Walsh JJ, Cooper DC *et al.* Mesolimbic
1043 dopamine neurons in the brain reward circuit mediate susceptibility to social defeat and
1044 antidepressant action. *J Neurosci* 2010; **30**(49)**:** 16453-16458.
1045 60. Eder P, Poteser M, Romanin C, Groschner K. Na(+) entry and modulation of Na(+)/Ca(2+)
1046 exchange as a key mechanism of TRPC signaling. *Pflugers Arch* 2005; **451**(1)**:** 99-104.
1047 61. Inoue R, Mori Y. Molecular candidates for capacitative and non-capacitative Ca2+ entry in
1048 smooth muscle. *Novartis Found Symp* 2002; **246:** 81-90; discussion 221-227.
1049 62. Nishida M, Watanabe K, Sato Y, Nakaya M, Kitajima N, Ide T *et al.* Phosphorylation of TRPC6
1050 channels at Thr69 is required for anti-hypertrophic effects of phosphodiesterase 5 inhibition.
1051 *J Biol Chem* 2010; **285**(17)**:** 13244-13253.
1052 63. Nishioka K, Nishida M, Ariyoshi M, Jian Z, Saiki S, Hirano M *et al.* Cilostazol suppresses
1053 angiotensin II-induced vasoconstriction via protein kinase A-mediated phosphorylation of the
1054 transient receptor potential canonical 6 channel. *Arterioscler Thromb Vasc Biol* 2011; **31**(10)**:**
1055 2278-2286.
1056 64. Su M, Li L, Wang J, Sun H, Zhang L, Zhao C *et al.* Kv7.4 Channel Contribute to
1057 Projection-Specific Auto-Inhibition of Dopamine Neurons in the Ventral Tegmental Area.
1058 *Front Cell Neurosci* 2019; **13:** 557.
1059 65. McCall NM, Marron Fernandez de Velasco E, Wickman K. GIRK Channel Activity in Dopamine
1060 Neurons of the Ventral Tegmental Area Bidirectionally Regulates Behavioral Sensitivity to
1061 Cocaine. *J Neurosci* 2019; **39**(19)**:** 3600-3610.
1062 66. Qu N, He Y, Wang C, Xu P, Yang Y, Cai X *et al.* A POMC-originated circuit regulates
1063 stress-induced hypophagia, depression, and anhedonia. *Mol Psychiatry* 2020; **25**(5)**:**
1064 1006-1021.
1065
1066 67. Butterweck V. Mechanism of action of St John's wort in depression : what is known? *CNS*
1067 *Drugs* 2003; **17**(8)**:** 539-562.
1068 68. Burlet S, Tyler CJ, Leonard CS. Direct and indirect excitation of laterodorsal tegmental neurons
1069 by Hypocretin/Orexin peptides: implications for wakefulness and narcolepsy. *J Neurosci* 2002;
1070 **22**(7)**:** 2862-2872.
1071 69. Jan-Pieter, Konsman. The mouse brain in stereotaxic coordinates: Second Edition (Deluxe) By
1072 Paxinos G. and Franklin, K.B.J., Academic Press, New York, 2001, ISBN 0-12-547637-X.
1073 *Psychoneuroendocrinology* 2003.
1074

1075
1076

1077 **Figure legends**

1078 **Fig.1** The effects of extracellular Ca^{2+} and Na^{+} on firing activity of the VTA DA
1079 neurons.

1080 **A**. Identification of the VTA DA neurons. i: confocal images showing the anatomical
1081 distribution of DA neurons in the VTA and SNc; the DA neurons were identified to be
1082 DAT-immunofluorescence positive (magnification,10X; scale bar, 100 μm). ii:
1083 single-cell PCR results; four cells showed the presence of genes indicated. **B**. The
1084 effect of replacing extracellular Ca^{2+} with Mg^{2+} on firing frequency of the VTA DA
1085 neurons. Example time-course (i) and traces (ii) of the spontaneous firing before and
1086 after replacement of extracellular Ca^{2+} (2 mM) by an equimolar amount of Mg^{2+}. iii:
1087 Summarized data for ii. Firing of the VTA DA neurons were recorded using loose
1088 cell-attached patch from a brain slice of the VTA (n=6). **C**. The effect of replacing
1089 extracellular Ca^{2+} with Mg^{2+} on the resting membrane potential (RMP) of the VTA
1090 DA neurons, in the presence of 1 μM TTX. Example time-course (i) and summarized
1091 data (ii) for the resting membrane potential before and after replacement of
1092 extracellular Ca^{2+} (2 mM) by an equimolar amount of Mg^{2+} (n=6). **D.** i: Replacement
1093 of external Na^{+} by equimolar NMDG resulted in hyperpolarization of the resting
1094 membrane potential of the VTA DA neurons, in the presence of 1 μM TTX. ii:
1095 Summarized data for i (n=5). Paired-sample T test, *** $P < 0.001$, ** $P < 0.01$, * $P <$
1096 0.05, n.s. $P > 0.05$. n is number of neurons recorded.

1097 **Fig. 2** Gene expression profile of non-selective cation channels (NSCCs) in the VTA
1098 DA neurons.

1099 Single-cell RNA-Seq was performed on the VTA neurons projecting to five different
1100 brain regions of mice (NAc c, NAc ms, NAc ls, BLA, mPFC). **A**. Gene expression
1101 profile of markers for neuron subtypes from 45 VTA neurons; the neuron subtypes
1102 included: dopaminergic (Th, Ddc DAT), GABAergic (Gad1, Gad2, VGAT) and
1103 glutamatergic (VGluT2, VGluT1, VGluT3), which was arranged in different rows
1104 indicated in the right labels and in the left-colored vertical lines; projection targets of
1105 these neurons were indicated at the top by the colored lines and labels. Relative
1106 expression levels of these genes were indicated by the dark-blue color intensity which
1107 was transformed from the log2 values of the number of transcripts per million (FPKM)
1108 plus 1. **B**. Relative gene expression levels of TRP channels (i) and other NSCCs (ii) in
1109 45 individual VTA DA neurons and the population average (mean, right columns).

1110 Each column of the individual neurons in (i) and (ii) corresponded to the columns in
1111 A. (iii) Bar graph of the mean log2 (FPKM +1) for the top 8 NSCCs in descending
1112 order. Error bars indicate SEM.**C.** Gene expression profile of aforementioned top 8
1113 NSCCs from 45 VTA neurons.

1114 **Fig. 3** NALCN contributes to subthreshold depolarization and spontaneous firing of
1115 the VTA DA neurons. **A**. Confocal images showing co-expression of NALCN (green)
1116 and DAT (red) representing DA neurons (scale bar, 10 μm). **B**. i: Single-cell PCR
1117 from the VTA DA neurons with the expression of NALCN. ii: Percentage of NALCN
1118 positive neurons from 15 DA neurons (with expression of DAT). **C**. Example time
1119 course (i) and summarized data (ii) showed that NALCN channel blockers ($GdCl_3$)
1120 significantly hyperpolarized the resting membrane potential (RMP) (n=5).
1121 Paired-sample T test, * $P < 0.05$. **D**. Example time-course and traces (i) and
1122 summarized data (ii) of the effect of $GdCl_3$ on spontaneous firing frequency in DA
1123 neurons (n=7). Paired-sample T test, ** $P < 0.01$. **E**. shRNA against NALCN
1124 carried by AAV virus (i) (NALCN-shRNA) was injected into the VTA of mice, the
1125 mRNA level in the shRNA-NALCN transfected VTA (NALCN-KD) and the scramble
1126 shRNA transfected VTA (Control) was analyzed using qPCR (ii) (n=6). Two-sample T
1127 test, ** $P < 0.01$. **F**. Confocal images showing the expression of
1128 AAV9-NALCN-shRNA-GFP (green) in the VTA DA neurons (DAT, red) (scale bar,
1129 10 μm). **G**. Loose cell-attached current clamp recordings of the spontaneous firing of
1130 the VTA DA neurons transfected with either NALCN-shRNA (n=12) or
1131 scramble-shRNA (Con, n=10) (both GFP and DAT positive). Examples of firing
1132 traces (i) and summarized data (ii) were shown. Two-sample T test, **** $P < 0.0001$.
1133 **H**. Whole-cell current clamp recordings of the resting membrane potential (RMP) of
1134 the VTA DA neurons transfected with either NALCN-shRNA (NALCN-KD, n=18) or
1135 scramble-shRNA (Con, n=15) (both GFP and DATpositive). Examples of firing traces
1136 (i) and summarized data (ii) were shown. Two-sample T test, **** $P < 0.0001$. n is
1137 number of neurons recorded.

1138 **Fig. 4** TRP channels contributes to subthreshold depolarization and spontaneous firing
1139 of the VTA DA neurons.

1140 **A**. The expression of TRP channels in VTA DA neurons. i: Single-cell PCR from 5
1141 VTA cells (C1-C5). ii: Percentage of TRP channels (C3, C6 and V2) positive neurons
1142 in the VTA DA neurons (DAT positive). **B** and **C**. Example time-course (i), traces (ii)

1143 and the summarized data (iii) for the effect of nonselective cation channel blockers
1144 2-APB (100 μM, n=12) (B), FFA (100 μM, n=13) (C) on the spontaneous firing
1145 frequency in the VTA DA neurons. B: Wilcoxon matched-pairs signed rank test, C:
1146 Paired-sample T test, *** $P < 0.001$. n is number of neurons recorded. **D** and **E.**
1147 Example time-course (i) and the summarized data (ii) for the effect of nonselective
1148 cation channel blockers 2-APB (n=6) (D), FFA (n=6) (E) in the resting membrane
1149 potential (RMP) of the VTA DA neurons. Paired-sample T test, ** $P< 0.01$. n is
1150 number of neurons recorded.
1151 **Fig. 5** TRPC6 contributes to subthreshold depolarization and spontaneous firing of the
1152 VTA DA neurons.
1153 **A**. The normalized expression profile of TRPC6 in NAc c and mPFC-projecting VTA
1154 DA neurons was verified using single cell-qPCR, (NAc c: n=28; mPFC: n=25, Both
1155 TH positive) Mann-Whitney U test, ** $P <0.01$. **B**. Confocal images showing
1156 co-expression of TRPC6 (green) and TH (red) representing DA neurons (scale bar, 10
1157 μm). **C**. The efficiency of shRNA knockdown of TRPC6 in the VTA verified by qPCR.
1158 Two-sample T test, ** $P <0.01$. shRNA against TRPC6 carried by AAV virus (i)
1159 (TRPC6-shRNA) was injected into the VTA of mice, the mRNA level in the shRNA-
1160 TRPC6 transfected VTA (TRPC6-KD) and the scramble shRNA transfected VTA
1161 (Con) was analyzed using qPCR (ii). **D**. Immunofluorescence labeling showing the
1162 expression of AAV9-shRNA(TRPC6)-GFP (green) and DAT (red) in the VTA (scale
1163 bar, 10 μm). **E**. Loose cell-attached current clamp recordings of the spontaneous firing
1164 of the VTA DA neurons from the mice transfected with either TRPC6-shRNA
1165 (TRPC6-KD, n=9) or scramble-shRNA (Con, n=9) (both GFP and DAT positive).
1166 Examples of firing traces (i) and summarized data (ii) were shown. Two-sample T test,
1167 ** $P < 0.01$. **F**. Example time-course (i) and summarized data (ii) showed that shRNA
1168 knockdown of TRPC6 in the VTA decreased the 2-APB-inhibited firing responses of
1169 the VTA DA neurons. (n=7, both GFP and DAT positive), Wilcoxon matched-pairs
1170 signed rank test, n.s. $P > 0.05$. **G**. Whole-cell current clamp recordings of the resting
1171 membrane potential (RMP) of the VTA DA neurons transfected with either
1172 TRPC6-shRNA (TRPC6-KD, n=10) or scramble-shRNA (Con, n=10) (both GFP and
1173 DAT positive). Examples of firing traces (i) and summarized data (ii) were shown.
1174 Two-sample T test, *** $P < 0.001$.
1175 **Fig. 6** CMUS depression mice have a decreased firing activity and downregulated

1176 TRPC6 expression in the VTA DA neurons.

1177 **A**. Experimental procedure timeline. **B**. i: Sucrose preference test for CMUS mice.
1178 Mann-Whitney U test, *** $P < 0.001$, compared with control mice. ii: Tail suspension
1179 test for CMUS mice, Two-sample T test, *** $P < 0.001$, compared with control mice.
1180 **C**. Loose cell-attached current clamp recordings of the spontaneous firing of the VTA
1181 DA neurons from the CMUS (n = 28 cells, DAT positive) and the control (n = 18 cells,
1182 DAT positive) mice. Mann-Whitney U test, **$P < 0.01$. **D**. Representative Western
1183 blot assay (i) and summarized data (ii) showing the expression of TRPC6 and
1184 GAPDH in the VTA of the control (Con) and the CMUS mice. Two-sample T test, **
1185 $P < 0.01$. n is the number of mice used. **E**. i and ii: Example time-course (up) and
1186 traces (bottom) showing the characteristic firing responses of 2-APB-inhibited
1187 mPFC-projecting VTA DA neurons in Con (i) and CMUS (ii) groups. iii. The effects
1188 of TRP channel inhibitor (2-APB) on the spontaneous firing activity of the
1189 mPFC-projecting VTA DA neurons in the control (n = 12 cells, DAT positive) and
1190 CMUS (n = 15 cells, DAT positive) mice. One-way repeated measures ANOVA with
1191 Dunnett's multiple comparisons test, n.s. $P > 0.05$, * $P < 0.05$, *** $P < 0.001$. iv. The
1192 inhibition rate (%) on firing rate by 2-APB in the control group (n = 12) and the
1193 CMUS group (n = 15). Mann-Whitney U test, *** $P < 0.001$.

1194 **Fig. 7** Selective knockdown of TRPC6 in the VTA DA neurons produces
1195 depression-like and anxiety-like behaviors and selective overexpression of TRPC6 in
1196 the VTA DA neurons rescues the TRPC6-knockdown-mediated depression-like and
1197 anxiety-like behaviors.

1198 **A**. shRNA against TRPC6 carried by AAV-loxp virus (TRPC6-shRNA) was injected
1199 into the VTA of the DAT-Cre mice. **B**. The mRNA level in the shRNA-TRPC6
1200 transfected VTA (TRPC6-cKD) and the scramble shRNA transfected VTA (Con) was
1201 analyzed using qPCR (Con: n=4; TRPC6-cKD: n=6). Mann-Whitney U test, * $P <$
1202 0.05. **C**. Immunofluorescence labeling showing the expression of
1203 AAV9-hSyn-DIO-shRNA(TRPC6)-RFP (red) and DAT (green) in the VTA of the
1204 DAT-Cre C57BL/6 mice (scale bar, 10 μm). **D**. The effects of Cre-induced conditional
1205 knockdown of TRPC6 in the VTA on the behaviors of mice in the sucrose preference
1206 test (i), the tail suspension test (ii), and the elevated plus-maze test (iii) (Con: n=9;
1207 TRPC6-cKD: n=13). Two-sample T test, ** $P < 0.01$, *** $P < 0.001$. **E**.
1208 AAV9-DIO-TRPC6-GFP was injected into the VTA of the DAT-Cre mice, 7 days after

injection of AAV9-hSyn-DIO-shRNA(TRPC6)-RFP . **F**. The protein level in the AAV9-DIO-TRPC6-GFP transfected TRPC6-cKD VTA (TRPC6-cKD+TRPC6-cOE) and the scramble RNA transfected Con and TRPC6-cKD VTA (Con and TRPC6-cKD) was analyzed using Western blot (Con: n=7; TRPC6-cKD: n=8; TRPC6-cKD+TRPC6-cOE: n=7). Kruslal-Wallis-H test with Dunnett's multiple comparisons test, $^{**}P < 0.01$. **G**. Immunofluorescence labeling showing the expression of AAV9-hSyn-DIO-shRNA(TRPC6)-RFP (red), AAV9-DIO-TRPC6-GFP (green) and DAT (blue) in the VTA of the DAT-Cre C57BL/6 mice (scale bar, 10 μm). **H**. The effects of Cre-induced conditional overexpression of TRPC6 in the VTA on the selective-knockdown-TRPC6-induced depression-like behaviors of mice in the sucrose preference test (i), the tail suspension test (ii), and the elevated plus-maze test (iii) (Con: n=11; TRPC6-cKD: n=11; TRPC6-cKD+TRPC6-cOE: n=11). One-way ANOVA with Dunnett's multiple comparisons test, $^{*}P < 0.05$, $^{**}P < 0.01$, $^{***}P < 0.001$.

Fig 1

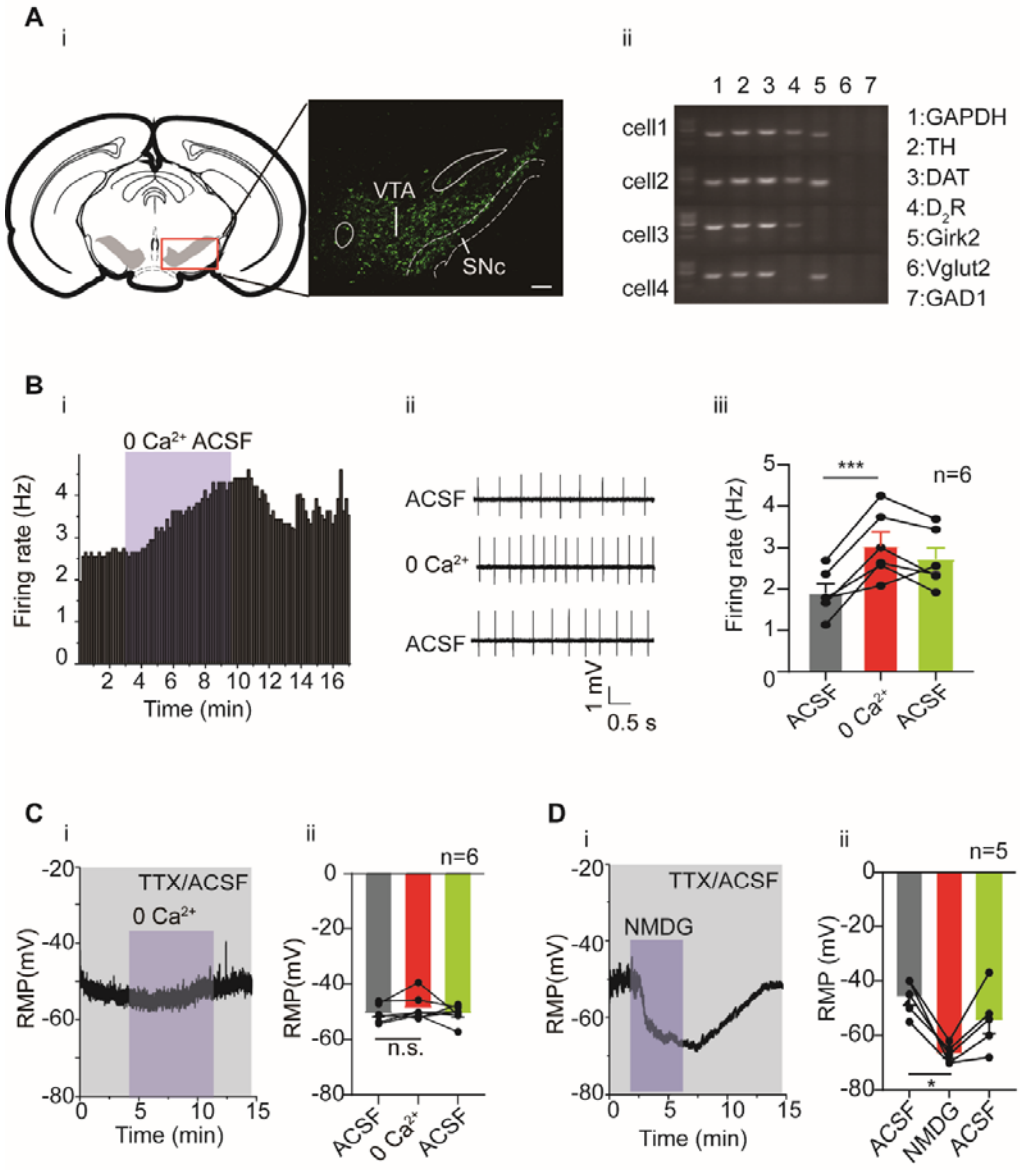

1225

1226

Fig 2

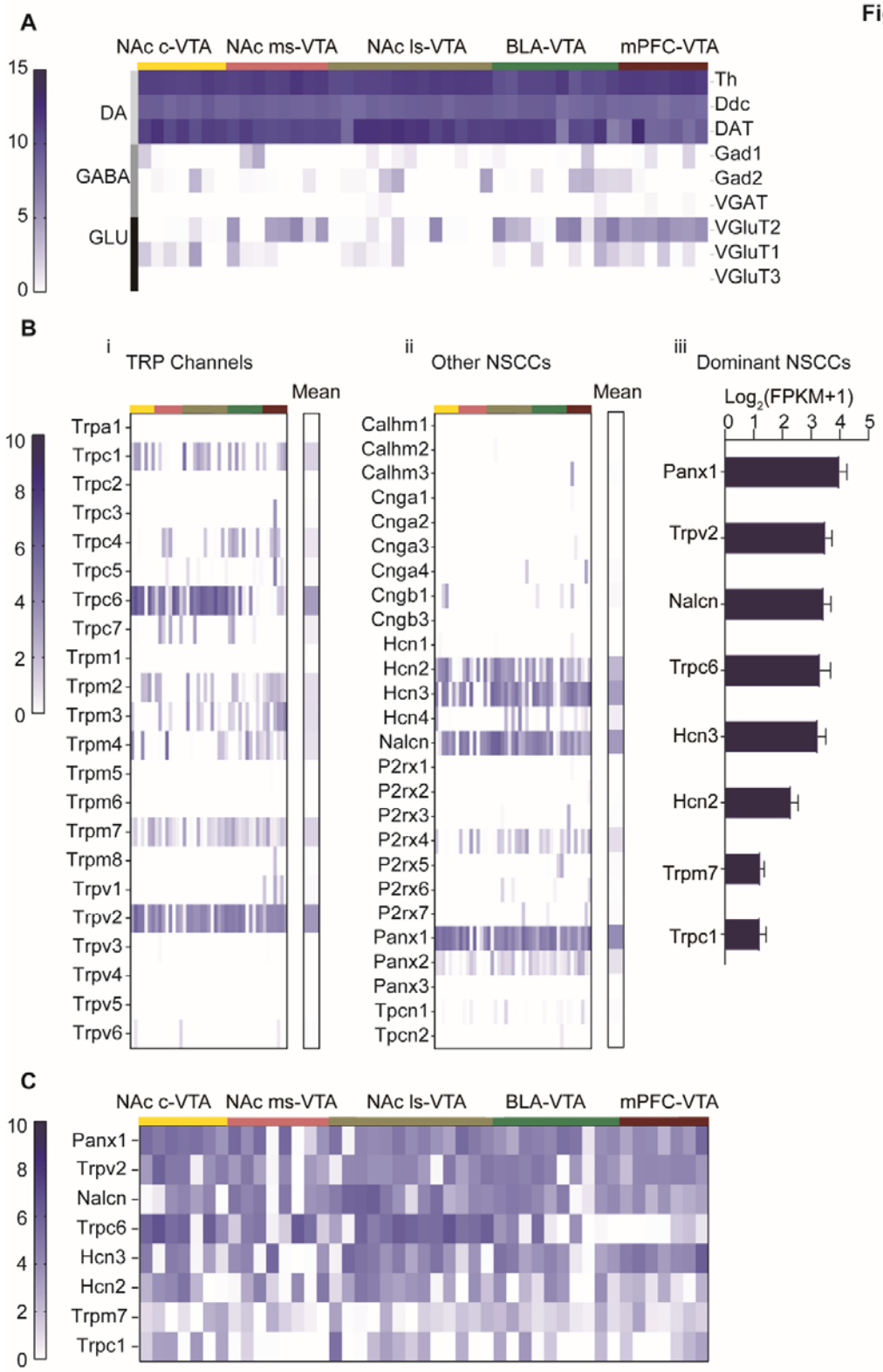
A
NAc c-VTA
NAc ms-VTA
NAc ls-VTA
BLA-VTA
mPFC-VTA
DA
GABA
GLU
Th
Ddc
DAT
Gad1
Gad2
VGAT
VGluT2
VGluT1
VGluT3
B
i TRP Channels
ii Other NSCCs
iii Dominant NSCCs
Mean
Log2(FPKM+1)
Trpa1
Trpc1
Trpc2
Trpc3
Trpc4
Trpc5
Trpc6
Trpc7
Trpm1
Trpm2
Trpm3
Trpm4
Trpm5
Trpm6
Trpm7
Trpm8
Trpv1
Trpv2
Trpv3
Trpv4
Trpv5
Trpv6
Calhm1
Calhm2
Calhm3
Cnga1
Cnga2
Cnga3
Cnga4
Cngb1
Cngb3
Hcn1
Hcn2
Hcn3
Hcn4
Nalcn
P2rx1
P2rx2
P2rx3
P2rx4
P2rx5
P2rx6
P2rx7
Panx1
Panx2
Panx3
Tpcn1
Tpcn2
Panx1
Trpv2
Nalcn
Trpc6
Hcn3
Hcn2
Trpm7
Trpc1
C
NAc c-VTA
NAc ms-VTA
NAc ls-VTA
BLA-VTA
mPFC-VTA
Panx1
Trpv2
Nalcn
Trpc6
Hcn3
Hcn2
Trpm7
Trpc1

Fig. 3

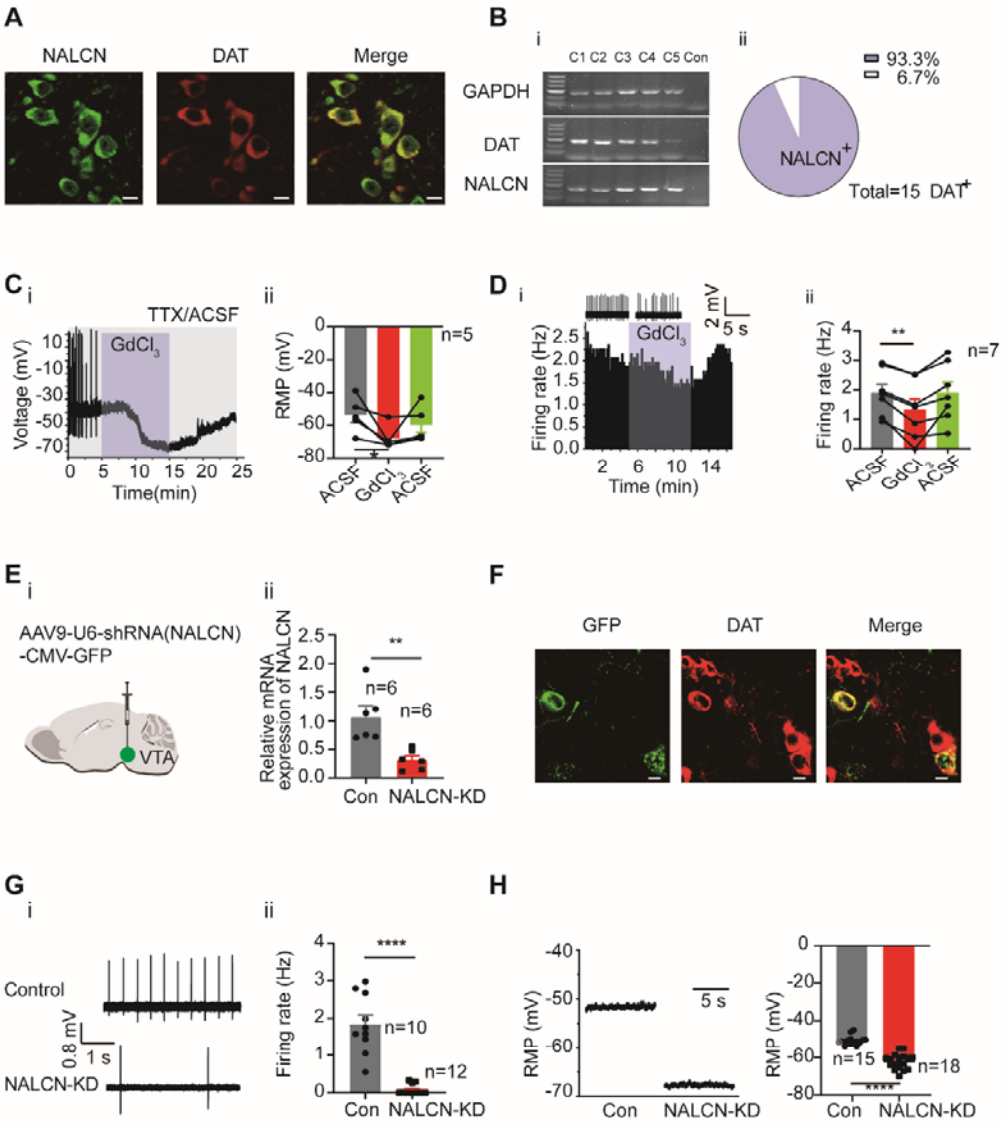
A
NALCN
DAT
Merge
B
i
C1 C2 C3 C4 C5 Con
GAPDH
DAT
NALCN
ii
93.3%
6.7%
NALCN+
Total=15 DAT+
C
i
TTX/ACSF
GdCl3
Voltage (mV)
Time(min)
ii
RMP (mV)
n=5
ACSF
GdCl3
ACSF
D
i
GdCl3
2 mV
5 s
Firing rate (Hz)
Time (min)
ii
**
n=7
Firing rate (Hz)
ACSF
GdCl3
ACSF
E
i
AAV9-U6-shRNA(NALCN)
-CMV-GFP
VTA
ii
Relative mRNA expression of NALCN
**
n=6
n=6
Con
NALCN-KD
F
GFP
DAT
Merge
G
i
Control
0.8 mV
1 s
NALCN-KD
ii
Firing rate (Hz)
****
n=10
n=12
Con
NALCN-KD
H
RMP (mV)
5 s
Con
NALCN-KD
RMP (mV)
n=15
n=18
****
Con
NALCN-KD

1229

Fig. 4

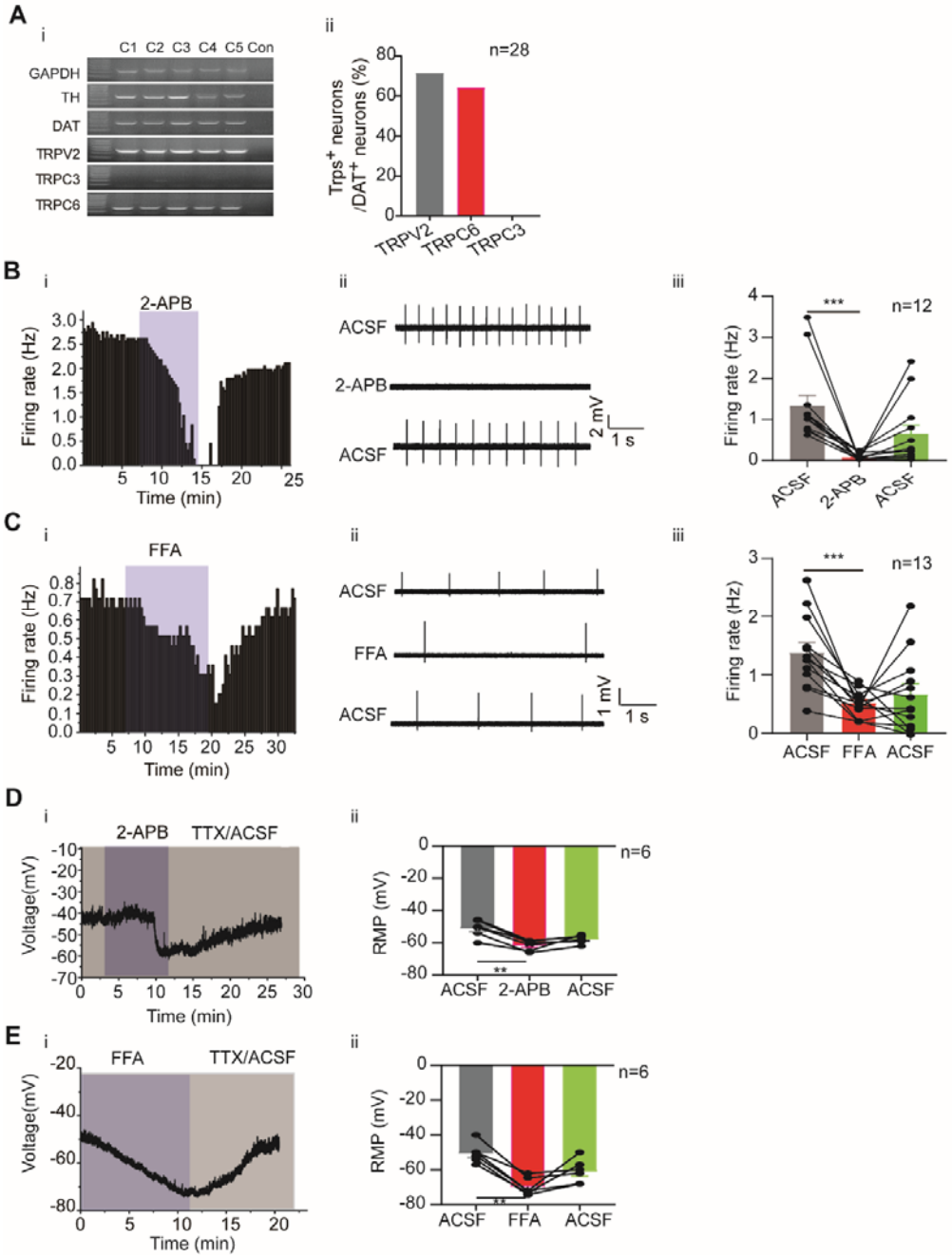
A
i
C1 C2 C3 C4 C5 Con
GAPDH
TH
DAT
TRPV2
TRPC3
TRPC6
ii
n=28
Trps+ neurons /DAT+ neurons (%)
TRPV2
TRPC6
TRPC3
B
i
2-APB
Firing rate (Hz)
Time (min)
ii
ACSF
2-APB
ACSF
2 mV
1 s
iii
***
n=12
Firing rate (Hz)
ACSF
2-APB
ACSF
C
i
FFA
Firing rate (Hz)
Time (min)
ii
ACSF
FFA
ACSF
1 mV
1 s
iii
***
n=13
Firing rate (Hz)
ACSF
FFA
ACSF
D
i
2-APB
TTX/ACSF
Voltage(mV)
Time (min)
ii
n=6
RMP (mV)
**
ACSF
2-APB
ACSF
E
i
FFA
TTX/ACSF
Voltage(mV)
Time (min)
ii
n=6
RMP (mV)
**
ACSF
FFA
ACSF

Fig. 5

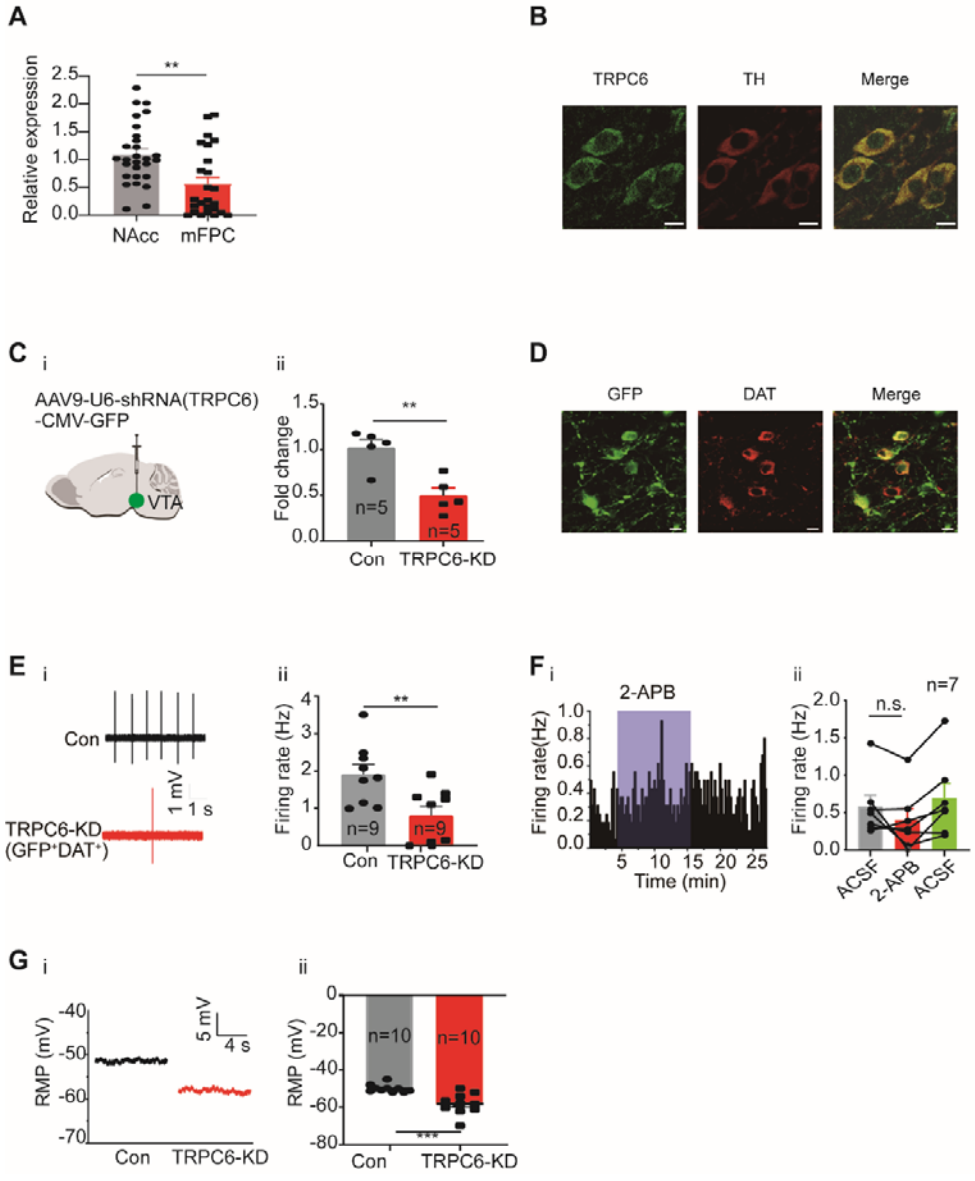
A
Relative expression
2.5
2.0
1.5
1.0
0.5
0.0
**
NAcc
mFPC
B
TRPC6
TH
Merge
C
i
AAV9-U6-shRNA(TRPC6)
-CMV-GFP
VTA
ii
Fold change
1.5
1.0
0.5
0.0
**
n=5
n=5
Con
TRPC6-KD
D
GFP
DAT
Merge
E
i
Con
1 mV
1 s
TRPC6-KD
(GFP+DAT+)
ii
Firing rate (Hz)
4
3
2
1
0
**
n=9
n=9
Con
TRPC6-KD
F
i
2-APB
Firing rate(Hz)
1.0
0.8
0.6
0.4
0.2
0.0
5
10
15
20
25
Time (min)
ii
n=7
n.s.
Firing rate (Hz)
2.0
1.5
1.0
0.5
0.0
ACSF
2-APB
ACSF
G
i
RMP (mV)
-40
-50
-60
-70
5 mV
4 s
Con
TRPC6-KD
ii
RMP (mV)
0
-20
-40
-60
-80
n=10
n=10
***
Con
TRPC6-KD

Fig. 6

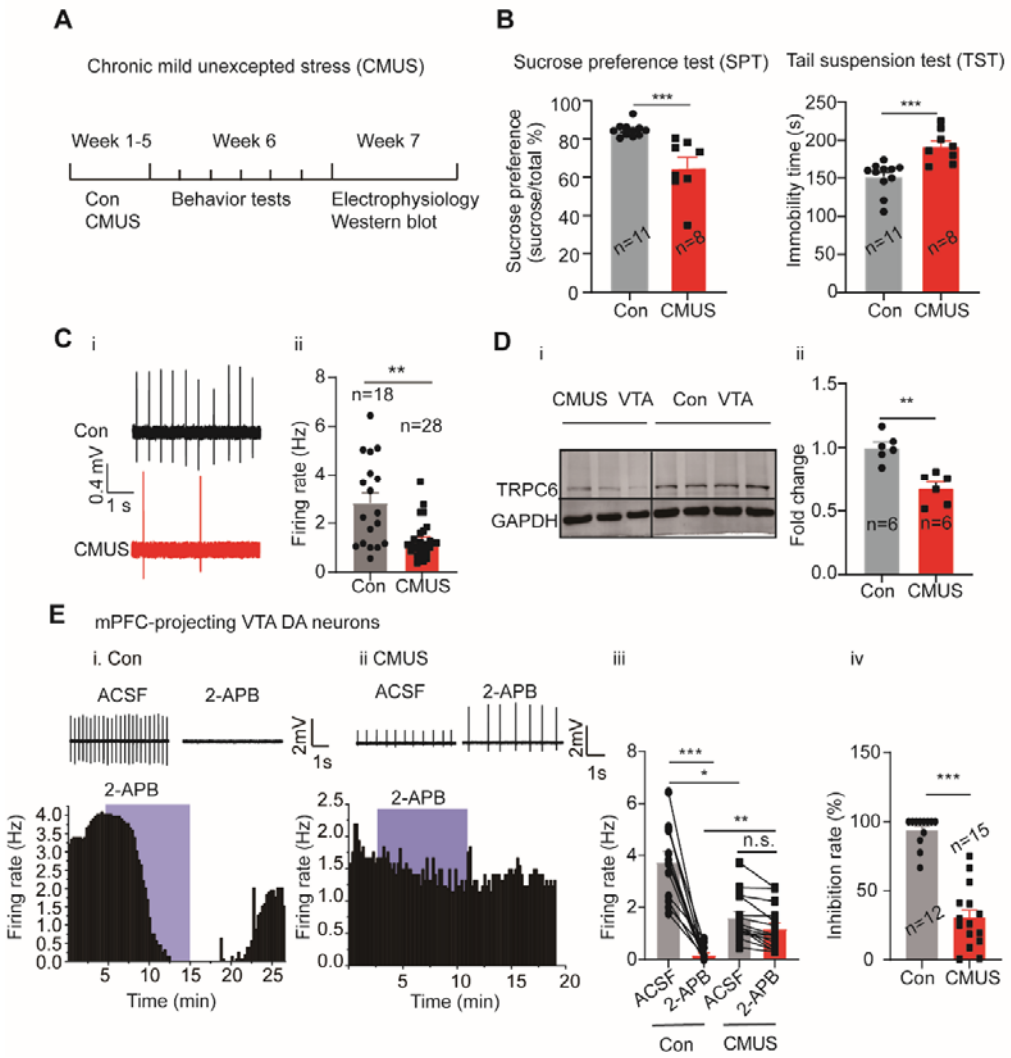

1234

1235

Fig 7

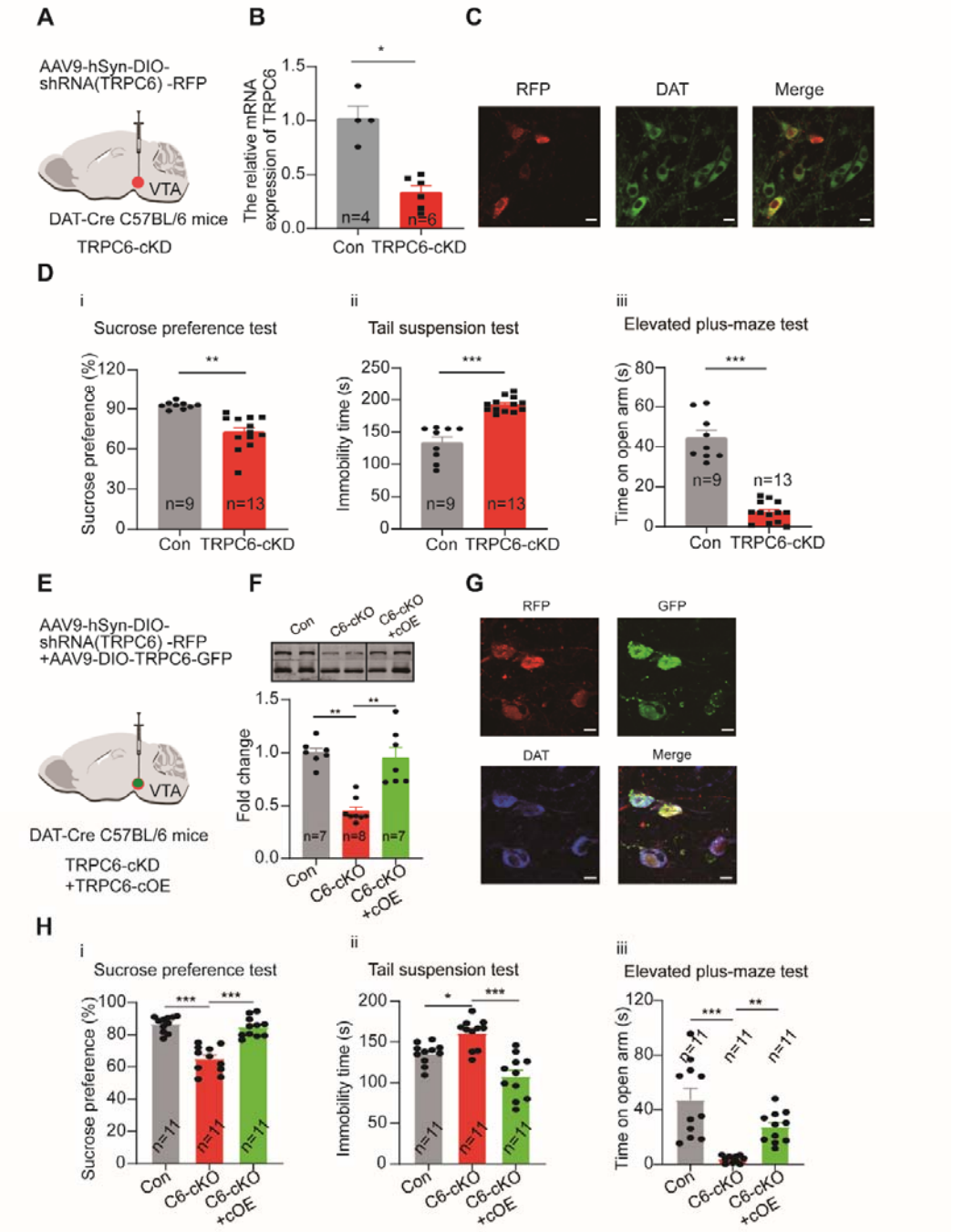
A
AAV9-hSyn-DIO-shRNA(TRPC6) -RFP
VTA
DAT-Cre C57BL/6 mice
TRPC6-cKD
B
The relative mRNA expression of TRPC6
n=4
n=6
Con TRPC6-cKD
C
RFP
DAT
Merge
D
i
Sucrose preference test
Sucrose preference (%)
n=9
n=13
Con TRPC6-cKD
ii
Tail suspension test
Immobility time (s)
n=9
n=13
Con TRPC6-cKD
iii
Elevated plus-maze test
Time on open arm (s)
n=9
n=13
Con TRPC6-cKD
E
AAV9-hSyn-DIO-shRNA(TRPC6) -RFP +AAV9-DIO-TRPC6-GFP
VTA
DAT-Cre C57BL/6 mice
TRPC6-cKD +TRPC6-cOE
F
Con
C6-cKO
C6-cKO +cOE
Fold change
n=7
n=8
n=7
Con
C6-cKO
C6-cKO +cOE
G
RFP
GFP
DAT
Merge
H
i
Sucrose preference test
Sucrose preference (%)
n=11
Con
C6-cKO
C6-cKO +cOE
ii
Tail suspension test
Immobility time (s)
n=11
Con
C6-cKO
C6-cKO +cOE
iii
Elevated plus-maze test
Time on open arm (s)
n=11
Con
C6-cKO
C6-cKO +cOE

1236